Thesis for the Degree of Doctor of Philosophy

Utilizing solar energy for anti-icing road surfaces using hydronic heating pavement with low temperature

Raheb Mirzanamadi

Department of Architecture and Civil Engineering
Division of Building Technology

CHALMERS UNIVERSITY OF TECHNOLOGY
Gothenburg, Sweden, 2019

Utilizing solar energy for anti-icing road surfaces using hydronic heating pavement with low temperature

Raheb Mirzanamadi

ISBN: 978-91-7597-854-3

Doktorsavhandlingar vid Chalmers tekniska högskola
Series number: 4535
ISSN no. 0346-718X

Department of Architecture and Civil Engineering
Division of Building Technology
Chalmers University of Technology
SE- 412 96 Göteborg
Sweden
Telephone: +46(0)31-772 1000

Cover:
Separation of the numerical simulation model of the hydronic heating pavement into two sub-models to obtain the minimum required energy for anti-icing the road surface.

Chalmers Reproservice
Göteborg, Sweden 2019

To Hoda

Utilizing solar energy for anti-icing road surfaces using hydronic heating pavement with low temperature

Raheb Mirzanamadi
Department of Architecture and Civil Engineering
Division of Building Technology
Chalmers University of Technology

Abstract

During summer, the surface temperature of an asphalt road pavement can rise up to 70°C due to absorbed solar radiation. The high temperature degrades the performance of the asphalt concrete by accelerating the thermal oxidation and plastic deformation, especially under heavy traffic loads. On the contrary, during winter, the temperature of road surfaces can reduce below the temperature of the ambient air due to the radiative heat loss. The low temperature hardens the asphalt pavement and makes it more susceptible to thermal cracking. Moreover, the low temperature causes the road surface to get slippery and hereby increases the risk for traffic accidents. A potentially environmental-friendly method to overcome the abovementioned problems is to use a Hydronic Heating Pavement (HHP). The HHP system consists of embedded pipes in the road. A fluid as thermal energy carrier circulates through the pipes. During sunny days, when the road surface is warm, the energy is harvested and saved in seasonal thermal energy storages. During cold days, the warm fluid from the storage is pumped back to the pipes to increase the surface temperature.

The aim of this study is to investigate the feasibility of the HHP system for harvesting solar energy during summer and anti-icing the road surface during winter. The study is done in five different steps: (i) determining the thermal properties of three typical asphalt concrete used for the construction of roads in Sweden using experimental tests and numerical simulation models, (ii) developing a 2D numerical simulation model of the HHP system to find out the most suitable boundary condition equations associated with the heat transfer interactions between the road surface and surrounding climate as well as the initial results related to the required energy for anti-icing the road surface and remaining number of hours of the slippery condition on the road surface, (iii) developing a hybrid 3D numerical simulation model of the HHP system to obtain the fluid temperature decline along the pipes and the effects of the fluid flow rate on the performance of the HHP system, (iv) calculating the minimum required energy for anti-icing the road surface using optimization tools so no slippery condition remains on the road surface and (v) investigating the feasibility of the coupled HHP system to a Horizontal Ground Heat Exchanger (HGHE) for harvesting solar energy and anti-icing the road surface. The numerical simulation model of the HHP system is made based on the finite element method and validated by the experimental results and analytical solutions as well as by the results of the other numerical simulation models from literature.

The results associated with the thermal properties show that the thermal conductivity of asphalt concrete can vary from 1 W/(m·K) to 3 W/(m·K). The results associated with the 2D numerical simulation model shows that the annual required energy for anti-icing is about 75 $\mathrm{kWh/(m^2 \cdot year)}$ and the remaining number of hours of the slippery condition after heating the road surface is 128 hours. The results associated with the hybrid 3D numerical simulation model show that the annual required energy for anti-icing is about 84 $\mathrm{kWh/(m^2 \cdot year)}$ and the remaining number of hours of the slippery condition after heating the road surface is 217 hours. The results associated with the optimization show that the minimum annual required energy for anti-icing the road surface is 107 $\mathrm{kWh/(m^2 \cdot year)}$ which results in remaining only 3 hours of the slippery condition on the road surface. Furthermore, the results associated with the coupled HHP system to the HGHE show that the annual required energy for anti-icing is about 75 $\mathrm{kWh/(m^2 \cdot year)}$ and the remaining number of hours of the slippery condition is 580 hours.

Key words: asphalt concrete; anti-icing; solar energy; optimization; ground heat exchanger

Användning av solenergi för att eliminera frosthalka från vägytor genom vattenbaserat vägvärmesystem med låg temperatur

Raheb Mirzanamadi
Arkitektur och samhällsbyggnadsteknik
Byggnadsteknologi
Chalmers Tekniska Högskola

Sammanfattning

Under sommartid kan temperaturen på asfaltbelagda vägar stiga upp till 70 ˚C. Den höga temperaturen accelererar den termiska oxidationen och kan leda till deformation, särskilt vid hög trafikbelastning. Å andra sidan, under vintertid kan temperaturen på vägar minska ner till omgivande luftens temperatur. Den låga temperaturen kan leda till att vägar blir hala och därmed ökar risken för trafikolyckor. En potentiellt miljövänlig metod för att minska ovannämnda problemen är att använda ett vattenbaserat vägvärmesystem system (HHP). HHP-systemet består av rör integrerade i vägbanan. En vätska cirkulerar genom rören som värmeenergibärare. Under sommartid utvinns solenergi och sparas in i ett termiskt säsongsenergilager. Under vintertid förs den energin tillbaka från det termiska energilagret till vägen för att öka vägytans temperatur.

Syftet med denna avhandling är att undersöka möjligheterna för att använda HHP-systemet till att utvinna solenergi under sommaren och minska risken för frosthalka under vintern. Avhandlingen består av fem delar: (i) experimentella tester och numeriska simuleringsmodell av asfalt, (ii) en 2D numerisk simuleringsmodell av HHP-systemet, (iii) en hybrid 3D numerisk simuleringsmodell av HHP-systemet, (iv) beräkning av minimienergi för att helt eliminera frosthalka från vägytan och (v) en simuleringsmodell av ett HHP system kopplat till en horisontell markvärmeväxlare. Den numeriska simuleringsmodellen av HHP-systemet valideras mot experimentella resultat och analytiska lösningar samt mot resultat från andra numeriska simuleringsmodeller från litteraturen.

Resultaten relaterade till asfaltens egenskaper visar att värmeledningsförmågan av asfaltbetong kan variera från 1 W/(m·K) till 3 W/(m·K). Resultaten relaterade till den numeriska 2D simuleringsmodellen visar att den årliga energin för att minska frosthalka är 75 $\mathrm{kWh/(m^2 \cdot year)}$ och det årliga återstående antalet timmar med frosthalka efter uppvärmning av vägytan är 128 timmar. Resultaten relaterade till den numeriska hybrid 3D simuleringsmodellen visar att den årliga energin för att minska frosthalka är 84 $\mathrm{kWh/(m^2 \cdot year)}$ och det återstående antalet timmar med frosthalka är 217 timmar. Resultaten relaterade till minimienergin visar att den årliga energi som krävs för att helt eliminera frosthalka är 107 $\mathrm{kWh/(m^2 \cdot year)}$ vilket leder till att endast 3 timmar med frosthalka återstår på vägytan under ett år. Dessutom visar resultaten relaterade till HHP-systemet kopplat till en horisontell markvärmeväxlare att den årliga energin för att minska frosthalka är 75 $\mathrm{kWh/(m^2 \cdot year)}$ och det återstående antalet timmar med frosthalka är cirka 580 timmar.

Nyckelord: asfalt; halkfria vägar; solenergi; optimering, markvärmeväxlare

Preface

PhD is a journey. For me this journey was not only to reach to the destination, it was whole the way to learn. Four and a half years with full of different experiences, happiness and events. The journey started in the 19th of August 2014 in a rainy and cloudy day in Gothenburg. The weather which was very close to what I was supposed to work on through my PhD project: "anti-icing the road surface". The only very simple problem was that I did not understand the project title very well for the first two years so as I went to a wrong path of "snow-melting" rather than "Anti-icing". From 19th of November 2016 to 7th of March 2017 when I defended my licentiate, I tried to find out the right path and since then I had two more years to steer the PhD project to the destination.

The Project has been financed by the Norwegian Public Road Administration (Statens vegvessen) for the first two and half years and then by Chalmers University of Technology for the last two years. A lot of people helped me in this project, including Dr. Jan Englund and Dr. Erick Oscarsson, from Skanska (Road Construction Company) in Gothenburg, who provided asphalt samples and gave advices about asphalt concrete, Dr. Henrik Karlsson from Bengt Dahlgren company who provided advice about optimization problems and Mr. Marek Machowski who helped with technical issues in the laboratory of Chalmers University of Technology.

I want to thank all my colleagues at the division of Building Technology for a good working environment and being good friends, especially Babak Ebrahimi, Alex Wunderlich and Ali Karim who were great friends. I also want to show my gratitude to Josef Johnsson, Pepe Tan and Fredrik Domhagen for being good friends and for the stimulating discussions over scientific problems. I want to especially thank Prof. Sotrios Grammatikos from NTNU who was a big help for me to write my first journal paper.

I would like to express my sincerest gratitude to my main supervisor, Prof. Carl-Eric Hagentoft for his trust, endless patience and super deep knowledge. I could not think of anyone better as a supervisor than he was. He is a role model for me scientifically and, very important, personally. Furthermore, I would like to say thanks to my co-supervisor: Assis. Prof. Pär Johansson who taught me professionality and helped me a lot with writing papers.

I would like to direct my special thanks to my family and parents, Shahnaz and Yousef, for their support and all they gave me to be whom I am now.

Last but not least, I would like to say very special thanks to my beautiful wife, Hoda, for everything from being the source of power to unconditional love. Many thanks for your support and patient for all those moments which were belong to you, but I was working.

Raheb Mirzanamadi
Gothenburg, January 2019

Notations and abbreviations

Symbol	Description	Unit
a	Thermal diffusivity	m^2/s
c	Distance between pipes	m
c_p	Specific heat	J/(kg·K)
d_{bore}	Depth of borehole	m
D	Embedded depth of pipes from its center to surface	m
DIA	Diameter	m
E	Annual energy	kWh/(m^2·year)
h_c	Convective heat transfer coefficient	W/(m^2·K)
h_e	Latent heat of water evaporation	kJ/kg
h_{eq}	Equivalent heat transfer coefficient	W/(m^2·K)
h_r	Radiation heat transfer coefficient	W/(m^2·K)
H	Depth	m
I	Solar irradiation	W/m^2
l	Characteristic length	m
L	Length	m
m	Mass per square meter	kg/m^2
$\dot{m}$	Mass flux per square meter	$kg/(m^2 \cdot s)$
M	Mass	Kg
Nu	Nusselt number	-
p	Water vapor partial pressure	Pa
Pr	Prandtl number	-
q	Heat flux	W/m^2
$\overline{q}_{p-year}$	Annual average of heat fluxes from pipe in road	W/m^2
q_s	Heat rate of borehole	W/m
$\overline{q}_{s-year}$	Annual average of heat rate of borehole	W/m
R_0	Thermal resistance between the pipes and surface	m·K/W
r and R_{pipe}	Pipe radius	m
R_s	Surface thermal resistance	m^2·K/W
Re	Reynolds number	-
RH	Relative Humidity	%
$S.D.$	Standard deviation	-
t	Time	s
T	Temperature	K, °C
$\overline{T}_{eq}$	Annual average of equivalent temperature	K, °C
T_{limit}	Criterion for turning on harvesting operation	K, °C
T_{max}	Annual maximum temperature at borehole wall	K, °C
T_{min}	Annual minimum temperature at borehole wall	K, °C
T.Diff	Mean temperature difference	K, °C
u	Moisture ratio (content) mass by mass	kg/kg
v	Velocity	m/s
V	Volume	m^3

$\dot{V}_f$	Fluid flow rate	$(\mathrm{l/min})$
W	Road width	m
x	Horizontal coordinate	m
y	Vertical coordinate	m
z	Height	m
z_0	Roughness lengths for momentum	m

Greek symbols	**Description**	**Unit**
β	Moisture transfer coefficient	m/s
v	Humidity by the volume	$\mathrm{kg/m^3}$
ε	Emissivity coefficient	-
λ	Thermal conductivity	W/(m·K)
ρ	Density	$\mathrm{kg/m^3}$
σ	Stephan-Boltzmann constant	$\mathrm{W/(m^2 \cdot K^4)}$
α	Absorptivity coefficient	-
ν	Kinematic viscosity	$\mathrm{m^2/s}$
u	Dynamic viscosity	$(\mathrm{kg/(m \cdot s)})$
κ	von Karman constant	-

Subscripts	**Description**
a	Air
ambient	Ambient air
con	Condensation
cond	Conductive heat transfer
conv	Convective heat transfer
dev	Deviation
dew	Dew-point
eq	Equivalent temperature/resistance
evp	Evaporation
f	Fluid
h	Harvested energy
i,j	Additional annulus surrounding the pipe
in	Inner/inlet
lw	Long wave radiation
loss	Heat loss
n	Number of sections
out	Outer/Outlet
p	Pipe/Periodic
PWS	Inner pipe wall surface
r	Required energy for anti-icing of the road surface
s	Saturated/surface
sw	Short wave radiation

List of papers

This thesis is based on the following papers which are appended:

Topic		Paper	Status
Thermal properties of asphalt concrete	I	**Mirzanamadi. R**., Johansson. P., Grammatikos. S. A., "Thermal properties of asphalt concrete: a numerical and experimental study". *Journal of Construction and Building Materials*., Vol. 158 (2018), p. 774-785.	Published (Journal)
2D numerical simulation model of the HHP	II	**Mirzanamadi. R**. Hagentoft. C.E., Johansson. P., Johnsson. J., "Anti-icing of road surfaces using hydronic heating pavement with low temperature". *Journal of Cold Region Science and Technology*., Vol. 145 (2018), p. 106-118.	Published (Journal)
	III	**Mirzanamadi. R**. Hagentoft. C.E., Johansson. P., "Hydronic heating pavement with low-temperature: the effect of pre-heating and fluid temperature on anti-icing performance". *Cold Climate HVAC 2018. CCC 2018.,* Springer Proceedings in Energy. Springer, 2019.	Published (Conference)
Hybrid 3D numerical simulation model of the HHP	IV	**Mirzanamadi. R**. Hagentoft. C.E., Johansson. P., "Numerical investigation of harvesting solar energy and anti-icing road surfaces using a hydronic heating pavement and borehole thermal energy storage". *Energies*., Vol. 11 (2018), 3443.	Published (Journal)
	V	**Mirzanamadi. R**. Hagentoft. C.E., Johansson. P., "Parametric study of hydronic heating pavement for anti-icing road surfaces using a hybrid 3D numerical simulation model"., *Conference of IBPSA* – Italy 2-4 Sept. 2019, Submitted.	Submitted (Conference)
Minimum required energy for anti-icing	VI	**Mirzanamadi. R**. Hagentoft. C.E., Johansson. P., "An analysis of hydronic heating pavement to optimize the required energy for anti-icing"., *Applied thermal engineering.,* Vol. 144 (2018), p. 278-290.	Published (Journal)
Coupled HHP system to the HGHE	VII	**Mirzanamadi. R**. Hagentoft. C.E., Johansson. P., "Coupling a hydronic heating pavement to a horizontal ground heat exchanger for harvesting solar energy and heating road surfaces"., Submitted to a scientific journal.	Submitted (Journal)

Papers I-VII were planned and written by me in contribution with Carl-Eric Hagentoft, Pär Johansson, Sotirios Grammatikos (Paper I) and Josef Johnsson (Paper II). I performed the experimental measurements and made the numerical simulations models. The co-authors helped with discussion, reviewing the paper and making comments.

Four other publications by the author are:

Licentiate thesis

a) **Mirzanamadi, R;** (2017): Ice free roads using hydronic heating pavement with low temperature: Thermal properties of asphalt concretes and numerical simulations. Chalmers University of Technology, Gothenburg, Sweden, 2017:02, ISSN 1652-9146

Conference papers

b) Adl-Zarrabi, B; **Mirzanamadi, R**; Johnsson, J; Hydronic Pavement Heating for Sustainable Ice-free Roads; Transportation Research Procedia; 2016

c) Adl-Zarrabi, B; Ebrahimi, B; Hoseini, M; Johnsson, J; **Mirzanamadi, R**; Taljegard, M; Safe and Sustainable Coastal Highway Route E39; Transportation Research Procedia; 2016

d) Adl-Zarrabi, B; Johnsson, J; **Mirzanamadi, R**; Hydronic Pavement Using Low Temperature Borehole Thermal Energy Storage; The 2016 World Congress on Advances in Civil, Environmental and Materials Research (ACEM16), Jeju Island, Korea, August 28-September1, 2016

Table of contents

1. Introduction

This chapter presents: (i) background, (ii) problem definition, (iii) scope of the study, (iv) methodology, (v) limitations and (vi) reading guide.

1.1. Background

During summer months, the surface temperature of an asphalt road pavement can rise up to 70°C, due to absorbed solar radiation [1]. The high temperature of the road surface usually degrades asphalt concrete by accelerating the thermal oxidation and plastic deformation under traffic loads. In addition, the high temperature of the road creates environmental matters such as the Urban Heat Island (UHI) effect. The UHI is referred to as areas of a city which are considerably warmer than their surroundings [2]. Furthermore, cold weather in winter reduces the road surface temperature. Low temperatures harden the asphalt concrete and subsequently induce thermal cracks on the surface of the road. Also, cold weather leads to the formation of ice on the road surface. Icy conditions increase the risk of traffic accidents and causes transportation safety problems [3]. The number of traffic accidents on a snow/ice covered road in Sweden is approximately five times higher than that on a dry road surface [4]. Approximately 50% of all annual fatal accidents of passenger cars in Sweden occur on slippery conditions [5]. In rural roads of northern Sweden, the proportion of fatal accidents associated with snow/ice covered roads is about 90% [6].

The most common method for mitigation of the slippery conditions on the road surface is to distribute salt and sand [7]. Generally, there are three main goals for usage of salt and sand, namely: anti-icing, de-icing and anti-compaction of snow [8]. Anti-icing is an action to prevent the wet road from freezing, de-icing is an action to melt the existing ice/snow on the road surface and finally the anti-compaction is an action to prevent the snow from compacting into a hard crust [9]. In Scandinavian countries, annually about 0.6 million tons salt and 1.7 million tons sand are consumed for winter maintenance of roads [10]. Salting is mainly used for roads with high traffic volumes when the average annual daily traffic (AADT) ranges from 2,000 to 3,000 and sanding mainly used for the secondary road networks with less traffic volume [3]. Salting and sanding are not environmentally friendly methods for removing ice and snow from the road surface. Salting and sanding can result in the pollution of the ground and surface waters [11] as well as the corrosion of vehicles and road infrastructures [12]. Furthermore, there is a temperature limitation for usage of the salt and sand. The Scandinavian guidelines operate with a lower limitation of -8°C on the road surface for distributing the salt and sand [3]. For the surface temperature lower than -8°C, it is difficult to keep the salt concentration high enough to prevent the ice-formation on the road surface [3]. It should be also noted that the salt and sand agents could be lost from road surface due to wind, traffic and runoff [8]. Moreover, the delay in distribution of salt and sand could lead to traffic congestion and severe traffic accidents at the slippery surface [13].

An environmental-friendly method to overcome the abovementioned problems is to use a Hydronic Heating Pavement (HHP) [14]. The HHP system consists of embedded pipes inside the road. A fluid such as brine (solution of salt and water), oil or glycol-water circulates through the pipes [15]. The HHP system harvests solar energy during sunny days, stores it in a Seasonal

Thermal Energy Storage (STES) and releases heat for ice/snow melting during cold periods [16]. Harvesting solar energy during summer leads to a decrease in the temperature of the road surface. On the contrary, heating the road surface during winter leads to an increase in the surface temperature which in turn leads to a decrease in the remaining number of hours of the slippery condition on the road surface [17].

Ground Heat Exchanger (GHE) is one the most common STES methods for heating/cooling road surface [18]. The GHE can be used year-round, regardless of the variation of the ambient temperature [19,20]. There are two types of the GHEs: Vertical Ground Heat Exchangers (VGHE) and Horizontal Ground Heat Exchangers (HGHE) [21]. The VGHE consists of vertically buried boreholes, the depths of which varies from 30 m to 200 m [22]. However, the HGHE consists of horizontally laid pipe networks in a shallow depth of 1 m to 2 m [23]. Application of the VGHE and HGHE for heating/cooling system in a building showed that the VGHE has approximately 15% higher heating/cooling efficiency comparing to the HGHE [19]. However, the installation cost of VGHE is approximately 15% higher than that of HGHE [19]. The scheme of the HHP systems coupled to a VGHE and HGHE are shown in Figure 1-1.

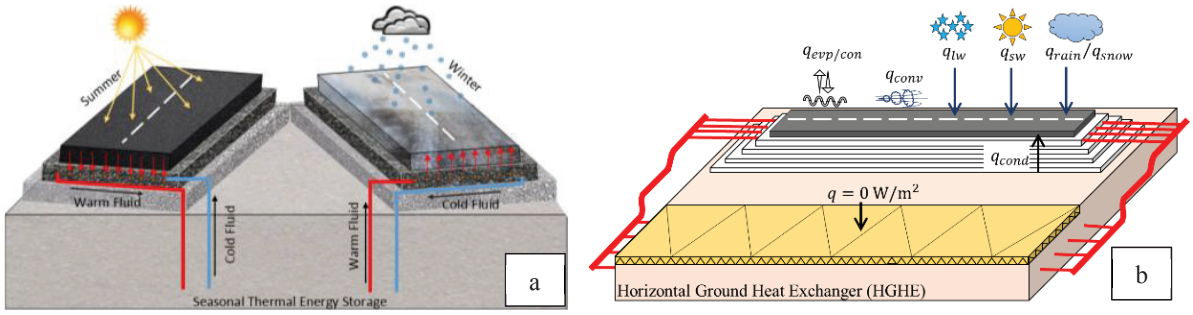

Figure 1-1. Scheme of a Hydronic Heating Pavement (HHP) system (a) the HHP system coupled to the Vertical Ground Heat Exchanger and (b) the HHP system coupled to the Horizontal Ground Heat Exchanger.

Installing the HHP systems in roads is not a new method. In 1948, the earliest system was installed in Klamath Falls in Oregon, USA by Oregon Highway Department. The source of energy in this system was geothermal hot water. This system failed after 50 years of working due to external corrosion of the metal pipes [24]. Another successful example for the HHP system is the SERSO project in Switzerland, installed on a bridge since 1994 [25]. The idea of the SERSO project was to defrost a bridge surface using renewable energies and guarantee the same road surface conditions on the heated bridge as on the subsequent road sections. The surface temperature of the bridge was set just above 0°C to prevent ice formation and freezing of compacted snow. The SERSO project was annually running approximately 1,000 hours in summer to harvest energy and another 1,000 hours in winter to alleviate the slippery conditions [26].

To analyze the anti-icing operation of the HHP system, different numerical simulation models were developed. Pahud [26] made a one-dimensional (1D) numerical model to simulate the heating system, installed in a bridge. This heating system was controlled using the air temperature. The heating system was turned on when the air temperature was below 4°C and turned off when the air temperature was below -8°C. The reason for turning off the system was the low likelihood of the ice formation on the road surface due to the low humidity content of

air for the air temperature below -8°C [27]. Moreover, Li *et al.* [28] examined two different heating systems to keep the surface temperature of the bridge higher than the freezing point of water. The first heating system was a simple ON/OFF system with a constant heating power and the second heating system was a dynamic heating system with a variable heating power. The dynamic heating system was developed based on an inverse heat conduction along the thickness direction of the bridge. Both the ON/OFF system and the dynamic heating system were able to keep the surface temperature of the bridge higher than 0.5 ℃. The required heat power for the ON/OFF system was constant of $206\ \mathrm{W/m^2}$, however, the maximum required heat power for the dynamic heating system was approximately $150\ \mathrm{W/m^2}$.

1.2. Problem definition

Although, previous studies [24,29] numerically simulated the HHP system and examined different parameters for heating the road surfaces, there are still some questions remaining. For example, previous studies mostly focused on the usage of the HHP system for snow-melting rather than anti-icing. The recommended fluid temperatures for snow-melting ranges from 25°C to 50°C [24]. This temperature range is high for the aim of anti-icing and will result in losing the energy which is required for heating the road surface. For the purpose of anti-icing, the control system for heating the road surface is a key point to decrease the energy consumption. Generally, two different strategies were used for anti-icing the road surface: (i) keeping the road surface temperature above 0 °C and (ii) keeping the road surface temperature above the dew-point temperature when the surface temperature is below 0°C. The annual required energy for anti-icing the road surfaces using the second strategy is 10 times less than that using the first strategy [30]. However, in the previous studies, the second strategy were combined with: either the constant fluid temperature [30] or the fluid temperature that varies based on the air temperature [26]. Those studies did not consider the time delay due to the heat conduction from the pipes to the road surface. This delay can result in remaining slippery conditions on the road surface.

Most of the previous numerical simulation models related to the heating and cooling of roads focus either on the HHP system [31] or on the GHE [22]. In addition, the studies associate with the HHP system were separated to either harvesting solar energy from the road surface [29] or heating the road surface [24]. There were few studies from literature that investigated the performance of the HHP system which is coupled to the GHE for both harvesting and heating periods. Even for these studies, the HHP system was coupled to the VGHE [26].

Moreover, the main part of heat in the HHP system is transferred through the road pavement. For the road pavement, constructed from the asphalt concrete, the thermal conductivity can vary between 0.7 W/(m·K) to 2.9 W/(m·K) [32,33]. However, in some of the previous studies associated with the HHP system, the thermal conductivity of asphalt layers were considered to be either too low, e.g. 0.7 W/(m·K) [34] or too high, e.g. 4 W/(m·K) [30]. Hence, the accurate determination of the thermal properties of asphalt concrete is essential for designing the HHP system.

1.3. Scope

The aim of this study is to investigate the performance of HHP system for harvesting solar energy during sunny days and anti-icing the road surface during cold periods. In the HHP system, the main part of the heat is transferred through the road materials. The thermal properties of three typical asphalt concretes, used to construct the road pavements in Sweden, are measured. Also, different design parameters of the asphalt concretes, such as aggregate types and air void contents, are examined to find out their effects on the thermal properties of asphalt concretes. Furthermore, the numerical simulation model of the HHP system is made to find out the influence of the different design options of the HHP system such as the fluid flow rate and fluid temperature on the required energy for anti-icing the road surface and the remaining number of hours of the slippery condition. The minimum required energy for anti-icing the road surface so that no slippery condition is remaining on the road surface is calculated. Moreover, the feasibility of the coupled HHP system to the Horizontal Ground Heat Exchanger (HGHE) are investigated for harvesting solar energy and anti-icing the road surface.

Examples of the research questions in this thesis are:

- What are the thermal properties of some typical asphalt concrete types used to construct different layers of the road such as wearing and binder layers in Sweden?
- How can different design components of an asphalt concrete such as aggregate types and air void contents influence the thermal properties of asphalt concretes?
- Can the HHP system with low fluid temperatures mitigate the slippery condition?
- What are the effects of design parameters of the HHP system such as inlet fluid temperature on the solar energy harvesting and anti-icing the road surface using the HHP systems?
- How can pre-heating the road surface affect the required energy for anti-icing the road surface using the HHP system and the remaining number of hours of the slippery condition?
- What is the minimum amount of required energy for anti-icing the road surface using the HHP system so that no slippery conditions remain on the road surface?
- What is the energy balance of the road surface during harvesting and anti-icing operations of the HHP systems which is coupled to the HGHE?

1.4. Methodology

In order to detect the thermal properties of the asphalt concretes, three different types of asphalt concrete (ABT11, ABS11 and AG22) were provided by the Skanska Road Construction Company in Gothenburg, Sweden. The delivered samples were some typical asphalt concrete types used in Sweden to construct asphalt bound layers (wearing, binder and base layers) of the road pavement structure. Thermal properties of asphalt concrete samples were measured using the Transient Plane Source (TPS) method. The accuracy of a measurement with the TPS method is highly dependent on the size of the employed sensor. Therefore, different measurements were taken using different TPS sensor sizes in order to investigate the effect of the sensor size vs. the maximum aggregate size ratio on the thermal property measurements. Moreover, a numerical simulation model of asphalt concrete was developed based on the random distribution programming to investigate the effects of different design parameters of asphalt concretes,

moisture and freezing conditions on the thermal properties of asphalt concrete. The generation process using random distribution programming was performed in MATLAB R2015b and COMSOL Multiphysics 5.2.

In order to analyze the harvesting and anti-icing operations of the HHP system, a 2D and a hybrid 3D numerical simulation models were developed. The 2D numerical simulation model was basis for developing the hybrid 3D numerical simulation model. The hybrid 3D model is represented by the 2D models which were connected to each other through the convective heat transfer of fluid. Both 2D and hybrid 3D numerical simulation models were used to examine the effects of different design options such as the distance between pipes and the diameter of pipes on the performance of the HHP system. Furthermore, the hybrid 3D numerical simulation model made it possible to investigate the effects of fluid flow rate on the performance of the HHP system and also check the fluid temperature rise along the pipes during the harvesting period and fluid temperature decline during the anti-icing period. Moreover, the hybrid 3D numerical simulation model was used to obtain the minimum required energy for anti-icing the road surface and also for studying the coupled HHP system to the HGHE. Furthermore, a 3D numerical simulation model of Borehole Thermal Energy Storage (BTES) were made to investigate the temperature change at the borehole walls on a long-term operation. The development of the numerical simulation models were done using COMSOL Multiphysics 5.3 and the optimization of the required energy was done based on a linear programming optimization using Gurobi Optimizer 7.5 [35], interfaced MATLAB R2016.b environment.

The climate data are obtained from Östersund (63.18 N and 14.5 E), a city in the middle of Sweden. The city has long and cold winter periods which makes it interesting to simulate the anti-icing operation of the HHP system. It should be noted that another main reason to use the climate data form Östersund was due to construction of a test site of the HHP system in this city. The annual mean temperature of the ambient air in Östersund is 2.53 °C [36]. The location of Östersund is shown in Figure 1-2.

Figure 1-2. Locations of Östersund in Sweden and Earth (Source: https://maps.google.com).

The 2D and hybrid 3D numerical simulation models were validated using (i) analytical solutions, (ii) an experimental test, (iii) a laboratory experimental test and (iv) the results of the numerical simulation models from two different literature.

Two analytical solutions were used to validate the 2D numerical simulation model. These two analytical solutions were related to: (i) thermal resistance between the pipe and the road surface and (ii) the heat flowing out from the pipe to the surrounding domain of the road. Furthermore, one analytical solution related to the decline of the fluid temperature along the pipes were used to validate the hybrid 3D numerical simulation model.

The experimental test was related to a road without embedded pipes from a test site in motorway E18 in Sweden [37]. The test site E18 is located in Sweden between the cities Västerås and Enköping. The data were selected because both climate data and measured temperature of the road, on the surface and at different depths, were available.

The laboratory experimental result related to the HHP system was taken from the literature [38]. The laboratory experimental test was selected because the boundary conditions on the road surface, the fluid temperature, the material properties and the average temperature on the road surface were known. The laboratory experimental test was used to validate the hybrid 3D numerical simulation model.

The hybrid 3D numerical simulation model in this study were compared with the results of the numerical simulation models from two different literature sources [39,40]. The numerical simulation models were selected because the boundary condition, the temperature of the surface, the material properties, the geometrical design as well as the inlet and outlet temperatures of fluid were known. The results from the other numerical simulation models were used to validate the hybrid 3D numerical simulation model.

1.5. Limitation

In this work, the asphalt concrete microstructure was 2D and created based on the assumption that the aggregates have cylindrical shape. The cylindrical shape of aggregates caused that the number of contact points between two aggregates to get only one point. However, if realistic aggregate shapes were used, the aggregate contact area would have been much larger which would have affected the heat transfer inside the asphalt concrete and the thermal properties of asphalt concrete. Another limitation associated with the numerical simulation of the asphalt concrete was the air void size. In this work, it was assumed that all air voids have the same sizes. However, in reality, the sizes of air voids are different.

Furthermore, in this study, it was assumed that all snowfalls were immediately removed from the road surface, so the investigation was not dealing with snow-melting and only the anti-icing performance of the HHP system was studied. Anti-icing in this study only referred to the prevention of ice-formation due to deposition of water vapor from the air to the road surface which better known as hoar frost formation [41]. Hence, the prevention of the ice-formation due to the wet surface and compacted snow were not investigated. Moreover, it was not taken into account that how thick of the ice on the road surface can cause the friction problem for driving. Furthermore, the anti-icing operation was only investigated for the first coming vehicle and then the effects of the produced heats from the vehicles engine, exhaust gases and traffic jam on the heat balances of the road surface were not taken into account.

Main part of this work was related to the road section and no storage section. Hence, an important limitation of the work was the interaction between the HHP system and the thermal energy storage. Only for one specific case; i.e. the coupled HHP system to the HGHE, the interaction between the road section and the storage section was investigated. However, for the coupled HHP system to the BTES, the road section and the storage section were decoupled from each other and their performance were investigated separately. Furthermore, the design of heat pumps was not investigated in this thesis.

Furthermore, the minimum required energy for anti-icing the road surface was based on the weather forecast for two next weeks. However, it was assumed that the weather forecast was 100% accurate and precise, so the reliability of the weather forecast was not examined.

In this work, it was assumed that there is no contact resistance between the pipes and the road materials and also there is no contact resistance between the different layers of the road. The road materials were considered to be made of asphalt concrete and so the cement concrete was not investigated. The emissivity and absorptivity values of the asphalt concrete were obtained from literature without measuring their values. These values were considered to be constant for all conditions during summer and winter.

1.6. Outline of the thesis

This thesis consists of a summery section and seven appended papers. The summery section consists of eight chapters including:

- Chapter 1 is about the background of the work, problem definition, scope of the thesis, methodology and limitation.
- Chapter 2 is about the determination of the thermal properties of the asphalt concrete using: (i) the experimental test (ii) the numerical simulation model of the asphalt concrete microstructure and (iii) the validation of the numerical simulation model of the asphalt concrete. This chapter is based on **Paper I**.
- Chapter 3 is about the 2D numerical simulation model of the HHP system, including (i) the mass and heat balance, (ii) the validation of the numerical simulation model using the experimental test and analytical solution, (iii) the numerical simulation model of the HHP system for Östersund case and (iv) the results related to the require energy for anti-icing the road surface and remaining number of hours of the slippery condition on the road surface. This chapter is based on **Papers II and III**.
- Chapter 4 is about the hybrid 3D numerical simulation model of the HHP system, including (i) the model development, (ii) the validation of the hybrid 3D numerical simulation model, (iii) the results related to the harvested solar energy, the require energy for anti-icing the road surface, the average outlet temperature of the fluid, the temperature reduction on the road surface during harvesting period and the remaining number of hours of the slippery condition on the road surface during anti-icing period as well as (iv) the long-term operation of the HHP system. This chapter is based on **Papers IV and V**.
- Chapter 5 is about the determination of the minimum required energy for anti-icing the road surface, including: (i) the superposition principle used for separation of the HHP system into two sub models, (ii) obtaining the elementary temperature response, (iii) the results related to the minimum required energy for anti-icing the road surface and (iv) running the full simulation model of the HHP system using the calculated minimum required energy. This chapter is based on **Papers VI**.
- Chapter 6 is about the investigation of the feasibility of the coupled HHP system to the HGHE, including (i) the model development, (ii) the feasibility the coupled HHP system to the HGHE for harvesting solar energy and anti-icing the road surface, (iii) the heat loss from the HGHE to the surrounding soil and (iv) the effects of the thermal properties of the

ground materials on the performance of the coupled system. This chapter is based on **Papers VII**.

- Chapter 7 is about the summary and conclusion from the work.
- Chapter 8 is about the possible suggestion for future work.

2. Thermal properties of asphalt concrete

This chapter presents: (i) experimental test to determine the thermal properties of the asphalt concrete (ii) numerical simulation model of the asphalt concrete microstructure and (iii) valuation of the numerical simulation model by the experimental results.

2.1. Experimental test to determine the thermal properties

There are several experimental methods to measure the thermal properties of asphalt concrete at ambient conditions [32,42]. The most common methods are steady-state, however, the measurement process by steady-state methods is time-consuming (up to several hours for each sample) [43]. Furthermore, setting up the steady-state conditions needs a specific size of asphalt concrete samples, depending on the measurement method. For example, the available guarded heat flow meter at Chalmers University of Technology requires sample size of 300 mm x 300 mm (sample thickness should be smaller than 70 mm). The available samples in this study were not large enough to use this method. In this study, instead, the Transient Plane Source (TPS) method was selected to measure the thermal properties of the asphalt concrete samples. The TPS method requires approximately 5 minutes to measure the thermal properties of materials.

The TPS method is based on a transiently heated plane sensor, made of a nickel double spiral. For a typical measurement, the sensor is located between two pieces of the (same) material. The TPS sensor is used both as a heating source and as a dynamic temperature sensor. Hence, an electric current is injected through the sensor and the generated temperature gradient between the two sample pieces is recorded. It is assumed that the sensor is located in an infinite medium. Therefore, the measurement time has to be controlled so that the thermal penetration depth does not exceed the thickness of the sample. It is worth noting that, by principle, the accuracy of the TPS method to determine the thermal conductivity of materials is within ±5% [44]. Further details on the TPS technique can be found in [44].

2.1.1. Asphalt concrete samples

Three different types of asphalt concrete (ABT11, ABS11 and AG22) which are some typical asphalt concrete types for construction of the road layers in Sweden were provided by Skanska Road Construction Company in Gothenburg, Sweden. The samples were manufactured in dimensions of 100 mm (diameter) x 60 mm (thickness). In all cases, three samples of the same asphalt concrete type were employed to measure the thermal properties. ABT11, ABS11 and AG22, on average of three samples, weighed 1,217 g, 1,151g and 1,169 g, respectively. Before testing, the samples were stored (pre-conditioning) for three weeks in room conditions e.g. 22℃ and 30% RH. The design parameters of each sample type are tabulated in Table 2-1. In particular, the (i) bitumen content, (ii) air content, (iii) asphalt concrete density, (iv) type of aggregate and (v) amount of aggregates passed from the different sieve sizes are depicted.

2.1.2. Influence of the TPS sensor size on the thermal properties values

In this study, the asphalt concrete samples were cut into halves. The thickness of each half sample is 30 mm±0.1 mm. The TPS sensor was then positioned between the two halves as shown in Figure 2-1 (a). Furthermore, Figure 2-1 (b) depicts the position of the TPS sensor on the surface of an asphalt concrete sample. The position of the TPS sensors between two clamped half samples of asphalt concrete were randomly selected to let the sensors acquire measurements

from different sample surface areas (e.g. binder, aggregate parts or their combination). Three measurements were recorded at each position and the mean value of the total six measurements was used as the thermal property of each sample. The waiting time between the two successive measurements was selected to be at least 20 min.

Table 2-1. Asphalt concrete samples parameters (data were provided by Skanska Road Construction Company).

ABT11			ABS11			AG22		
Bitumen content:5.8% Air content: 2.1% Bulk density: 2,617 kg/m^3			Bitumen content: 6.6% Air content: 2.8% Bulk density: 2,421 kg/m^3			Bitumen content: 4.1% Air content: 4.9% Bulk density: 2,582 kg/m^3		
Sieve size (mm)	Amount of passed aggregate %	Agg. type	Sieve size (mm)	Amount of passed aggregate %	Agg. type	Sieve size (mm)	Amount of passed aggregate %	Agg. type
31.5	100	Diabase	31.5	100	Quartzite	31.5	100	Diabase
22.4	100		22.4	100		22.4	97	
16	100		16	100		16	76	
11.2	98		11.2	96		11.2	57	
8	77		8	51		8	44	
5.6	62		5.6	36		5.6	37	
4	50		4	30		4	30	
2	34		2	25	Diabase	2	21	
1	24		1	19		1	15	
0.5	18		0.5	15		0.5	12	
0.25	14		0.25	14		0.25	9	
0.125	9		0.125	11		0.125	7	
0.075	7.9		0.075	9.6		0.075	5.7	

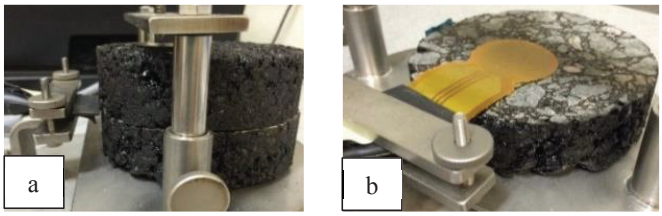

Figure 2-1. Using Transient Plane Source (TPS) method to measure the thermal properties of the asphalt concrete (a) employing the sensor between two halves samples and (b) the TPS sensor position on the surface of an asphalt sample. (Photos: Raheb Mirzanamadi)

The different TPS sensor sizes were employed to examine their effect on the measurement of thermal properties. Table 2-2 tabulates the (i) sensor ID, (ii) sensor diameter, (iii) injected power, (iv) measurement time related to each different sensor size and (v) thermal penetration depth. The penetration depth is calculated as $2 \cdot \sqrt{a \cdot t}$. Here, a (m^2/s) is the thermal diffusivity and t (s) is the measurement time [44].

Table 2-2. Details related to the measurement of the thermal properties of the asphalt concrete samples using the different TPS sensor sizes.

Sensor ID	Sensor diameter (mm)	Power (mW)	Measurement time (s)	Thermal penetration depth (mm)
5465	6.36	100	10	4-5
5501	12.8	200	40	8-10
8563	19.7	300	80	12-18
4922	29.2	1000	160	18-21
5599	58.8	1000	320	22-26

The effects of the sensor size vs. the maximum aggregate size ratio on the thermal conductivity and thermal diffusivity values are presented in Figure 2-2. Where each value represents the mean value of 18 measurements (3 [specimens] (x) 2 [positions] (x) 3 [times]). In the TPS method, the thermal conductivity is the actual and important result of the experiment. The accuracy of thermal diffusivity and volumetric heat capacity depends on the temperature increase (preferably greater than 1°C) and number of collected data points around the characteristic time, r^2/a (s). Where r (m) is the TPS sensor radius and a is the thermal diffusivity [44,45]. Dixon et al. [45] reported that the accuracy and repeatability of the thermal conductivity, measured by the TPS method is within ±2%. This value for the thermal diffusivity changes to ±10% [45].

As can be seen in Figure 2-2, when the sensor diameter to the maximum aggregate size ratio is less than 2, a significant variation between the measured thermal properties occurs. The use of small sensor sizes which cover small measuring areas, often leads to inaccurate measurements e.g. the thermal conductivity of AG22 is 25% higher when measured with a 6.36 mm diameter sensor compared to a 58.8 mm diameter sensor. It is highly likely that the thermal property readings when using the small-sized sensor (6.36 mm diameter) represent mostly the thermal properties of the aggregates. On the other hand, a large size sensor (58.8 mm diameter) is large enough to cover both aggregate and binder areas allowing for more rational measurements. By increasing the sensor size to the maximum aggregate size ratio, the variations in the measured thermal conductivity and diffusivity values are minimized. When this ratio exceeds 2, the variation of the thermal properties (apart from the thermal diffusivity of ABS11) is less than 4%. ABS11 consists of about 70% quartzite (coarse aggregate) and 30% diabase (fine aggregate), a non-uniform distribution of which might be the cause of the encountered oscillation in the thermal properties when using different sensors. In such design case, it is recommended to employ large size sensors. The sensor size with the diameter of 19.7 mm has a ratio of 1.7 in the case of ABS11. This implies the fact that only a single large quartzite aggregate can be fully covered by the sensor during a measurement. Sensor sizes with the diameters of 29.2 mm and 58.8 mm correspond to 2.65 and 5.45 ratios, respectively. Hence, they are large enough to cover 2 and 5 large quartzite aggregates, increasing the accuracy of the thermal property measurements.

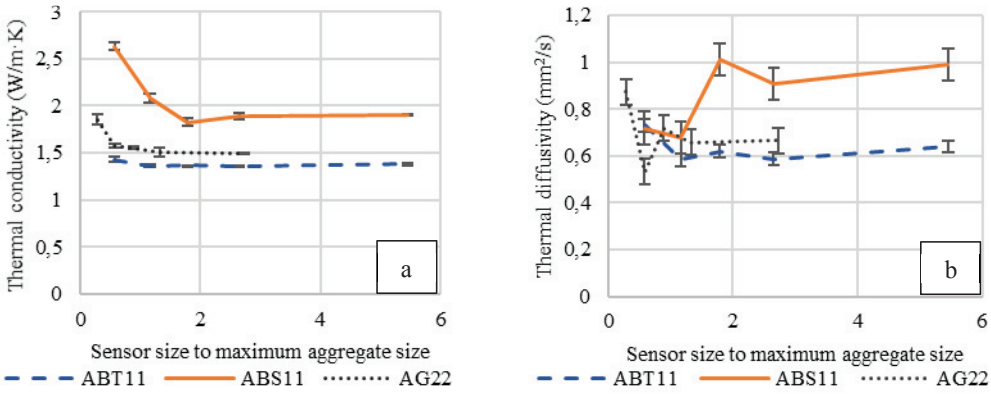

Figure 2-2. The effects of the ratio of sensor diameters to the maximum aggregate size on (a) the thermal conductivity and (b) the thermal diffusivity. The vertical bars show the standard deviations of 18 measurements.

2.2. Numerical simulation model of the asphalt concrete microstructure

A hierarchically-based multiscale approach was adopted as a common method to generate the microstructure of asphalt concrete. As such, the generated structure by smaller aggregates is regarded as a component of the next structure composed of larger aggregates e.g. the structure generated of bitumen and filler, aggregates smaller than 0.075 mm, is regarded as 'binder' for asphalt concrete composed of aggregates larger than 0.075 mm. Previous studies [46,47], as shown in Figure 2-3 (a), employed several matrices to generate the final asphalt sample to calculate thermal conductivity values. However, this process exhibited reduced accuracy in the computed results and required several simulation efforts. In this study, in order to increase the accuracy of the results (taking into consideration the improved contact and mechanical interlocking among different aggregates) and also reduce the simulation process efforts, the asphalt concrete microstructure (including all aggregate sizes larger than 0.075 mm in Table 2-1) is generated in only one numerical sample, see Figure 2-3 (b).

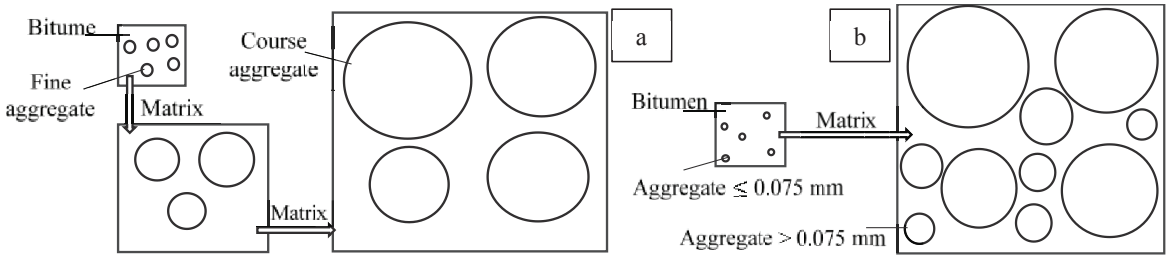

Figure 2-3. Scheme of generating aggregate microstructure using a hierarchical multiscale method (a) generating different matrix to reach the final sample (b) the generated microstructure model in this thesis using only one matrix

In this thesis, the method of random distribution programming was used to numerically generate the microstructure of asphalt concrete samples. The required time to generate the microstructure of the ABT11 sample, using random distribution programming, was approximately 5 min. It is worth noting that Chen et al. [46] reported that, when aggregates are randomly distributed, their aspect ratio does not significantly influence the thermal conductivity of asphalt concrete (less than 1%). Therefore, in this work, the shape of the aggregates was considered to have circular cross-sections. Furthermore, despite the fact that a real asphalt concrete sample is three-dimensional (3D), considering the required time consumption and computational resources of generating 3D models, this study followed a development of a 2D numerical model approach. It is also worth noting that, Chen et al. [46,47] showed that difference between the calculated thermal conductivity of the asphalt concrete using 2D and 3D numerical models is about 5%.

The generation process using random distribution programming was performed in MATLAB R2015b and COMSOL Multiphysics 5.2. Details are as follows:

I. The amount of different aggregates is calculated for a square of 90 mm side length size.

II. The generation of aggregates starts from the larger to the smaller size. To speed-up the process, after generating and randomly placing an aggregate, the placed area is booked and no more random aggregates can be generated and occupy the same place.

III. A control system is posed on generated aggregates to avoid overlapping with other aggregates. In the case of aggregate overlap, the aggregate position is removed and a new position is randomly selected. The process continues until zero overlapping.

After generating all aggregates, a square of 45 mm side length size is extracted from the generated area as the final sample. The reason of length downsizing is to reduce the effects of fine aggregate distribution (at the edges of the generated sample) on the thermal conductivity and also reduce the computational cost. The extracted sample length is two times larger than the larger possible aggregate size (22.4 mm), see Table 2-1. A representative numerically generated microstructure is shown in Figure 2-4.

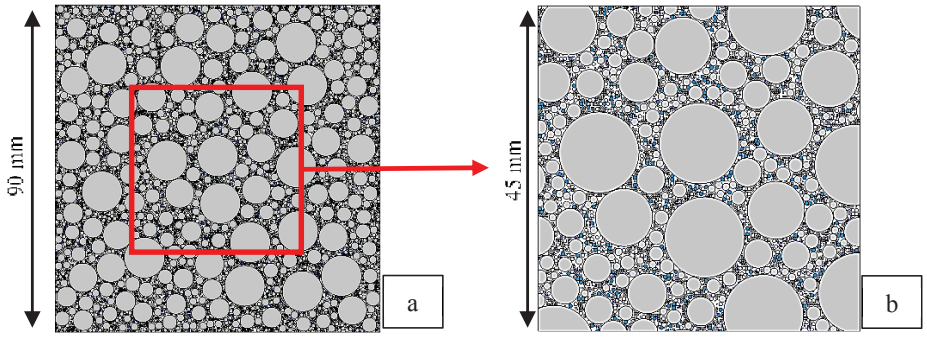

Figure 2-4. The numerically generated microstructure (a) initial generated asphalt concrete model and (b) final extracted asphalt concrete model to measure the thermal properties. Gray circles represent aggregates, blue circles represent air voids and white area represents the binder (bitumen and filler)

It should be noted that the downsizing of asphalt concrete model may affect the distribution of the different constituents. Table 2-3 illustrates the distribution of the constituents in the initial and final numerical models. As can be seen, downsizing results in more coarse aggregates in the final model.

Table 2-3. Volumetric distributions of asphalt concrete components in the initial and final numerical models.

Component	Volumetric distribution of components in the asphalt sample (%)					
	ABT11		ABS11		AG22	
	Initial model	Final model	Initial model	Final model	Initial model	Final model
Coarse aggregate	58.56	54.77	65.45	63.06	66.88	66.79
Fine aggregate	19.04	21.65	9.73	11.52	11.99	12.93
Air void	1.57	2.10	2.18	2.80	4.15	4.90
Binder (bitumen and filler)	20.83	21.48	22.63	22.62	16.98	15.38

2.3. Validation of the numerical model by experimental results

In the numerical model, the thermal properties of asphalt concrete are influenced by the distribution of components (coarse aggregate, fine aggregate, air void and binder) along with the volumetric fraction and the thermal properties of each component. The distribution and the volumetric fraction of the components are presented in Section 5 of **Paper I**. The thermal properties of the different constituents were derived from literature and used as input in the model. Table 2-4 lists the derived thermal properties of different components.

Table 2-4. Thermal properties of different components.

Reference	Component	Thermal conductivity (W/(m·K))	Density (kg/m^3)	Specific heat capacity (J/(kg·K))
Pen *et al.* 2014 [48]	Binder without additives	0.39	1459	1158
Theodore *et al.* 2011 [49]	Liquid water	0.61	1000	4181
	Stagnant air (22°C)	0.025	1.18	1017
	Ice (at -5°C)	2.25	918	2027
Côté *et al.* 2013 [32] Andofsson 2013 [50] Robertson 1988 [51]	Quartzite aggregate	4- 8 (Here 5 W/m·K is selected from [32])	2650	850
	Diabase aggregate	1.5- 2.5 (Here 2.3 W/m·K is selected from [32])	2980	817

Three samples were numerically generated for each type of asphalt concrete. The effective thermal conductivity, λ (W/(m·K)), for the asphalt concrete samples was calculated at steady-state and at two principal (perpendicular) directions. The details for calculation of thermal conductivity, thermal diffusivity and volumetric heat capacity are presented in Section 3-1 of **Paper I**.

The results associated with the thermal properties of asphalt concrete obtained through the experimental and numerical methods are tabulated in Table 2-5. The relative error is defined as the difference between the experimentally and numerically derived thermal properties, divided by the experimental values [relative error = (experimental value-numerical value)/experimental value]. As it is shown, the relative error is between 2% and 10%, which would suggest that the proposed numerical model is reliable enough to predict the thermal properties of asphalt concrete.

Table 2-5. Thermal properties of asphalt concrete obtained from numerical and experimental methods. (SD: Standard Deviation; Num.: Numerical model; Exp.: experimental testing, RE: relative error).

Thermal properties	ABT11			ABS11			AG22		
	Num.	Exp.	RE (%)	Num.	Exp.	RE (%)	Num.	Exp.	RE (%)
Thermal conductivity (W/(m·K))	1.37	1.39	1.44	1.84	1.89	2.65	1.39	1.51	7.94
S.D. for thermal conductivity (W/(m·K))	0.02	0.02	-	0.1	0.03		0.05	0.05	-
Volumetric heat capacity (MJ/(m^3·K))	2.23	2.16	3.24	2.11	2.08	1.44	2.31	2.25	2.67
S.D. for volumetric heat capacity (MJ/(m^3·K))	-	0.06	-	-	0.09		-	0.09	-
Thermal diffusivity (mm^2/s)	0.61	0.64	4.69	0.87	0.91	4.39	0.60	0.67	10.4
S.D. for thermal diffusivity (mm^2/s)	0.01	0.02	-	0.05	0.01	-	0.02	0.05	-

3. Two dimensional (2D) numerical simulation model

This chapter presents: (i) the mass and heat balance on the road surface, (ii) the validation of the numerical simulation model of the HHP system, (iii) the numerical simulation of the HHP system for Östersund and (iv) results.

3.1. Mass and heat balance

This section presents mass and heat balances of the road surface. The equations are derived from [52].

3.1.1. Mass balance

It is assumed that all snowfall is immediately removed from the road surface and rainfall is drained well. In this study, the mass balance of the road surface is based on condensation and evaporation as:

$$\frac{dm''_{moisture}}{dt} = \dot{m}''_{con} - \dot{m}''_{evp} \qquad (3\text{-}1)$$

$m''_{moisture}$ ($\mathrm{kg/m^2}$) is the mass balance of water on the road surface, t (s) is the time, $\dot{m}''_{con}$ ($\mathrm{kg/(m^2 \cdot s)}$) is the condensation rate to the surface and $\dot{m}''_{evp}$ ($\mathrm{kg/(m^2 \cdot s)}$) is the evaporation rate from the surface.

3.1.2. Heat balance

It is important to note that the heat flux associated with the latent heat of the snow melting is not considered in the heat balance due to the snow removal from the road surface. However, falling snow, before the snow removal is started, affects the heat balance of the road surface. Hence, the sensible heat flux of snow, q_{snow}, related to the heat capacity of snow is considered in the heat balance. As can be seen in Figure 3-1, the heat balance of the road surface consists of seven heat fluxes, including: conductive heat flow from ground and pipes, q_{cond}, convective heat flow from the ambient air, q_{conv}, sensible heat of rain, q_{rain}, sensible heat of snow, q_{snow}, long-wave radiation, q_{lw}, short-wave radiation, q_{sw}, as well as the latent heat of evaporation and condensation, $q_{evp/cond}$. The heat balance is written as:

$$q_{cond} + q_{conv} + q_{rain} + q_{snow} + q_{lw} + q_{sw} + q_{evp/con} = 0 \qquad (3\text{-}2)$$

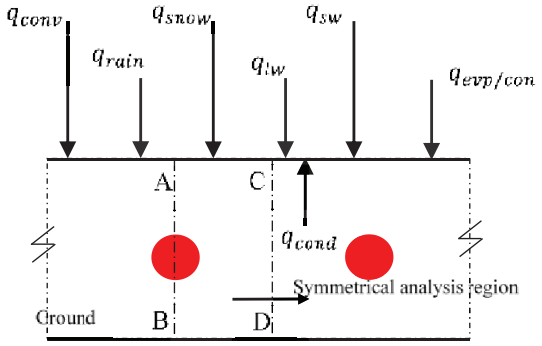

Figure 3-1. Heat balance of the road surface.

In Figure 3-1, all of the heat fluxes directed toward the road surface, however this does not mean that they are always positive. A positive sign (+) indicates that energy is given to the surface from the ambient and a negative sign (-) indicates that energy is taken out from the surface to the ambient.

Table 3-1 presents the details related to each heat flux. λ (W/(m·K)) is the thermal conductivity of the road materials (treated as constant by moisture and temperature variations), T (K) is the temperature, $T_{ambient}$ (K) is the ambient air temperature, $T_{surface}$ (K) is the road surface temperature, T_{sky} (K) is the sky temperature, ε (-) is the emissivity of the surface, α (-) is the solar absorptivity of the surface, σ ($W/(m^2 \cdot K^4)$) is the Stefan-Boltzmann constant, I (W/m^2) is the solar irradiation, h_c ($W/(m^2 \cdot K)$) is the convective heat transfer coefficient, h_e (J/kg) is the latent heat of evaporation of water, β (m/s) is the moisture transfer coefficient, $\rho_a c_{pa}$ ($J/(m^3 \cdot K)$) is the volumetric heat capacity of the ambient air at atmospheric pressure, $v_{ambient}$ (kg/m^3) is the humidity by the volume of the ambient air, v_s (kg/m^3) is the humidity by the volume of the saturated air at the surface temperature, $\dot{m}_{snow}$ ($kg/(m^2 \cdot s)$) is the snowfall rate per square meter of the surface, $\dot{m}_{rain}$ ($kg/(m^2 \cdot s)$) is the rainfall rate per square meter of the surface, c_{p-snow} ($J/(kg \cdot K)$) is the heat capacity of ice crystals in snow and $c_{p-water}$ ($J/(kg \cdot K)$) is the heat capacity of water.

Table 3-1. Different heat fluxes on the road surface.

Heat transfer process	Equation	No.
Conductive heat	$q_{cond} = -\lambda \cdot \nabla T$	3-3
Convective heat	$q_{conv} = h_c \cdot (T_{ambient} - T_{surface})$	3-4
Long-wave radiation	$q_{lw} = \varepsilon \cdot \sigma \cdot (T_{sky}^4 - T_{surface}^4)$	3-5
Short-wave radiation	$q_{sw} = \alpha \cdot I$	3-6
Evaporation/Condensation	$q_{evp/con} = h_e \cdot \beta . (v_{ambient} - v_s)$ where ($\beta = \frac{h_c}{\rho_a c_{pa}}$)	3-7
Sensible heat flux of snow	$q_{snow} = \dot{m}_{snow} \cdot c_{p-snow} \cdot (T_{ambinet} - T_{surface})$	3-8
Sensible heat flux of rain	$q_{rain} = \dot{m}_{rain} \cdot c_{p-water} \cdot (T_{ambient} - T_{surface})$	3-9

3.2. Validation of the numerical simulation model of the HHP system

This section presents the validation of the numerical simulation model for two cases: (i) the road without embedded pipes and (ii) the road with embedded pipes. For the first case, the validation is done using the measured data from an experimental test site in the motorway E18. For the second case, the validation is done using two different analytical solutions.

3.2.1. Validation of the numerical simulation model without embedded pipes using experimental data

In order to validate the numerical model, the motorway E18 [37] was chosen because both climate data and measured temperature of the road surface were available. The details related to the motorway E18 and the details of simulation are provided in Section 3-1 of **Paper II**. Only results related to the validation are provided in this section.

Figure 3-2 (a) illustrates the scatter plot of the calculated and measured temperature of the road surfaces for the test site E18 during the year 2014. In this Figure, the vertical axis, y (°C), represents the numerically calculated surface temperature and the horizontal axis, x (°C), represents the measured surface temperature. For the best case, y=x. In this study, the relation between y and x is obtained as: y=1.06·x-0.4°C.

Furthermore, Figure 3-2 (b) illustrates the calculated and measured road surface temperatures for October 2014. For this period, the mean temperature difference between the calculated and measured data (T.Diff.) is -0.13°C with the standard deviation (S.D.) of 1.93°C. Using different values for emissivity and absorptivity values of the road surface will lead to different results, see Table 2 in **Paper II.**

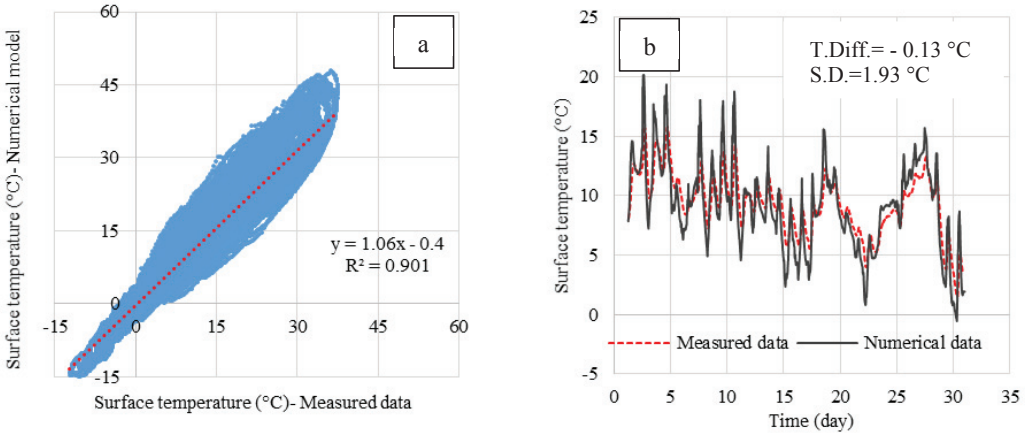

Figure 3-2. Comparing the surface temperatures obtained from the numerical simulation model and measured data of the test site E18 (a) the scatter plot of the calculated and measured temperatures (b) the surface temperature versus time for October 2014.

3.2.2. Validation of the numerical model with embedded pipes using analytical solution

Two different analytical solutions are used to validate the numerical simulation model with the embedded pipe. The analytical solutions are associated with: (i) the thermal resistance between the pipes and road surface and (ii) the heat flowing out from the pipe located in an infinite region.

(i) Analytical solution associated with the thermal resistance between the pipes and road surface

In this section, the thermal resistance between the pipes and road surface, R (m·K/W), is obtained from an analytical solution and the numerical model. The analytical solution represents the 2D thermal process in the cross-section of the road which is perpendicular to the pipe. It is assumed that the road material is homogenous. The thermal resistance is theoretically modeled for a single embedded pipe, located in the middle of an infinite array of pipes. The theoretical model is based on that the road domain is divided into strips with equal width and with adiabatic surfaces at the strip boundaries. The analytical solution accounts for the distance between the pipes, the embedded depth of the pipes, the pipe size, the thermal conductivity of materials and the surface thermal resistance. The equations related to the analytical solution are obtained from [53] and presented in Section 3-2 of **Paper II**. The scheme of the road section used for the analytical solution is shown in Figure 3-3.

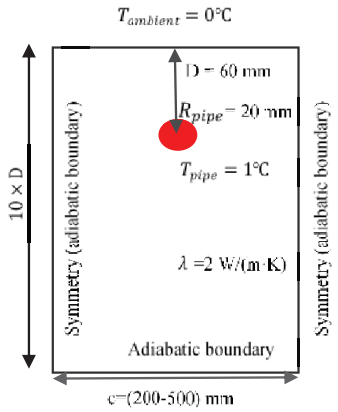

Figure 3-3. Road section used for the analytical solution related to thermal resistance between pipes and surface.

A pipe with the radius of 20 mm is embedded at the depth of 60 mm from the surface. The fluid temperature and the ambient temperature are set to be 1°C and 0°C, respectively. The road consists of one layer with the thermal conductivity of 2 W/(m·K). The analytical solution is based on a semi-infinite geometry. In the numerical simulation, the height of the model was truncated to 10 times the embedded depth of the pipe. The thermal resistance between the pipe and road surface is obtained from both the analytical solution and numerical model. The distances between the pipes varied from 200 mm to 500 mm. The surface resistance is considered to be 0.1 m^2·K/W.

The results associated with the thermal resistance between the pipes and the road surface are shown in Figure 3-4. As can be seen, the results of the thermal resistance between the pipe and surface related to the numerical model and analytical solution are matching well. The maximum relative error between two methods is 1%. It is worth noting that the analytical model is based on line sources and the error compared with real circular pipes increases when the pipes are too close to each other or too close to the ground surface.

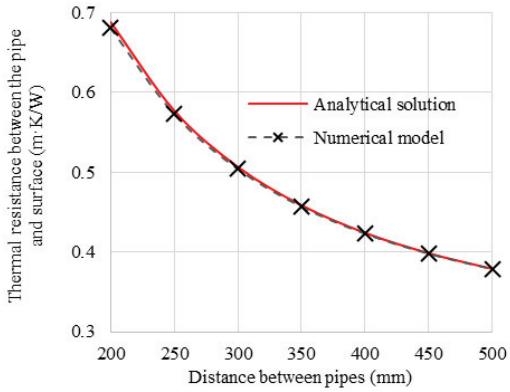

Figure 3-4. Thermal resistance between the pipe and surface for different pipe distances (the surface thermal resistance is 0.1 m^2·K/W).

(ii) Analytical solution associated with the heat flowing out from the pipe located in an infinite region.

This section presents the results associated with the heat flow, q (W/m), in an infinite region bounded internally by a pipe with a constant temperature, obtained from an analytical solution

and the numerical simulation. The equations related to the analytical solution are obtained from [54] and presented in Section 3 of **Paper III**.

A scheme of the model used for the analytical solution is shown in Figure 3-5.

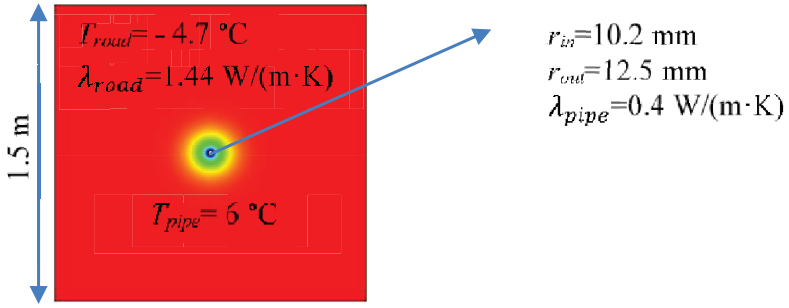

Figure 3-5. Scheme of the model used for analytical solution related to the heat flow from pipes.

A pipe with the inner radius of 10.2 mm and outer radius of 12.5 mm is embedded in a square area, side length of which is 1.5m. The size of the area is considered to be large enough in order to resemble the infinite region in the analytical solution. The fluid temperature is 6°C and the road temperatures is -4.7°C. The thermal conductivity of the pipe material is 0.4 W/(m·K) and that of the road material is 1.44 W/(m·K). The results associated with the heat flow, q (W/m), and energy loss, E (kWh/m) are shown in Table 3-2. As can be seen, the maximum relative errors related to the heat flow and energy loss between the analytical and numerical methods are 4% and 6%, respectively. The relative error for both heat flow and energy loss is less than 4% for when the running time is longer than 20 minutes.

Table 3-2. Comparison between analytical and numerical simulation.
Relative error= (Numerical result/Analytical result-1)×100.

	Heat flow, q (W/m)			Energy, E (kWh/m)		
Time (min)	Analytical solution	Numerical solution	Relative error (%)	Analytical solution	Numerical solution	Relative error (%)
10	46.063	47.883	3.95	0.0094	0.0099	5.64
20	40.321	41.400	2.68	0.0165	0.0171	3.58
30	37.442	38.357	2.44	0.023	0.0235	2.28
40	35.593	36.333	2.08	0.0291	0.0296	1.77
50	34.259	34.815	1.62	0.0349	0.0355	1.66
60	33.231	33.668	1.32	0.0405	0.0411	1.60
120	29.769	29.871	0.34	0.0718	0.0727	1.32

3.3. Numerical simulation model of the HHP system for Östersund

As mentioned in Section 1-4 of this thesis, the climate data were obtained from Östersund. The climate data included: dry-bulb/air temperature (°C), relative humidity (%), wind speed (m/s), dew-point temperature (°C), incoming long-wave radiation (W/m^2), short-wave radiation (W/m^2) and precipitation (mm/h). The numerical simulation was modeled using the implicit time-stepping method. The time-step was 1 hour in line with the resolution of climate data [36].

To start the investigation, an arbitrary geometry of the HHP system was selected for the simulation. The road structure consists of six different layers: the first three layers are made of asphalt concretes, the next second layers are made of crushed aggregates and the last layer is

ground. For more details see Section 3-1 of **Paper II.** Furthermore, in this thesis, it was assumed that the temperature of the ground at the depth of 5 m from the road surface was equal to the annual mean temperature of the ambient air. The data related to the road and pipes, used for the numerical simulation, are presented in Tables 3-3 and 3-4.

Table 3-3. Materials properties of the road layers [17].

Materials	Thickness (mm)	Thermal Conductivity (W/(m·K))	Density (kg/m^3)	Specific Heat Capacity (J/(kg·K))
Wearing layer	40	2.24	2415	848
Binder layer	60	1.44	2577	822
Base layer	100	1.51	2582	894
Subbase layer	80	0.7	1700	900
Subgrade layer	1000	0.8	1400	900
Ground	3720	0.6	1300	600

Table 3-4. Information about the simulated HHP system.

Parameter	**Value**	**Unit**
Thermal conductivity of pipe materials	0.4	W/(m·K)
Density of pipe materials	925	kg/m^3
Specific heat capacity of pipe materials	2300	J/(kg·K)
Outer diameter of the embedded pipes	25	mm
Pipe thickness	2.3	mm
Distance between the pipes	100	mm
Embedded depth (from center of the pipe to the surface)	87.5	mm
Emissivity of the road surface	0.89	-
Absorptivity of the road surface	0.78	-
Fluid Temperature	6	°C

Condensation occurs on the road surface if the surface temperature, $T_{surface}$, is lower than the dew-point temperature of ambient air, T_{dew}. If $T_{surface}$ is lower than the freezing temperature of water, $T_{freezing}$, then the moisture on the road will turn to ice. Therefore, if $T_{surface} < 0℃$, the HHP system is to keep the surface temperature above T_{dew} to avoid condensation. Moreover, to prevent ice formation on the road surface before the heating starts, the HHP system is turned on before that $T_{surface}$ is below $T_{freezing}$ and T_{dew}. In this case, even if the surface temperature is lower than the freezing temperature, ice is not formed on the road surface. The mentioned criteria for running the HHP system could be written as:

$$\begin{cases} T_{surface} < T_{dew} + \Delta T_{dew} \\ T_{surface} < T_{freezing} + \Delta T_{freezing} \end{cases} \text{ where } (\Delta T_{dew} \text{ and } \Delta T_{freezing}) \geq 0℃ \qquad (3\text{-}10)$$

where, $T_{surface}$ is the surface temperature in the middle between the pipes (point C in Figure 3-1). ΔT_{dew} and $\Delta T_{freezing}$ are the temperature thresholds for pre-heating (equal to or above 0°C) related to dew-point and freezing temperatures, respectively. Whenever the heating is started, the temperature of fluid, circulating through the pipes, is set to be 6°C. Furthermore, whenever the heating is stopped, the boundary condition at the inner surface of the pipe walls is set to be adiabatic. It should be noted that the temperature drop of the fluid along the pipe is

assumed to be negligible. By calculating the heat flow from a single pipe, $q_{pipe-heating}$ (W/m), the annual required energy for anti-icing the road surface, E_r (kWh/(m^2·year)), is calculated as:

$$E_r = \frac{1}{c} \cdot \int_{t=0}^{1\,year} q_{pipe-heating} \cdot dt \quad (3\text{-}11)$$

where c (m) is the distance between the pipes. Furthermore, the number of hours of the slippery condition on the road surface, $t_{slippery}$ (h), are calculated when the temperature of the road surface is lower than both $T_{freezing}$ and T_{dew}.

$$t_{slippery} = \int_{0}^{1\,year} f \cdot dt \quad (f = 1 \;\; if \begin{pmatrix} T_{surface} < T_{dew} \\ T_{surface} < T_{freezing} \end{pmatrix} \text{ else } \; f = 0) \quad (3\text{-}12)$$

Moreover, in order to investigate how different values of ΔT_{dew} and $\Delta T_{freezing}$ can affect the anti-icing performance of the HHP system, the parameter of *SR* (-) is defined as the relative difference of remaining hours of slippery condition, $\frac{t_{slippery\_inital} - t_{slippery}}{t_{slippery\_inital}}$ $(-)$ to the relative difference of annual required energy, $\frac{E_r - E_{r\_initial}}{E_{r\_initial}}$ $(-)$, see Equation 3-13. It should be noted that a higher value of *SR* means that a small increase in the annual required energy results in a large reduction in the remaining slippery hours of the road surface.

$$SR = \frac{\frac{t_{slippery\_inital} - t_{slippery}}{t_{slippery\_inital}}}{\frac{E_r - E_{r\_initial}}{E_{r\_initial}}} \quad (3\text{-}13)$$

3.4. Results

Table 3-5 presents the results of anti-icing the road surface for $\Delta T_{dew} = 0$℃ and $\Delta T_{freezing} = 0$℃ . As can be seen, 75.3 kWh/(m^2·year) energy is annually required to mitigate the slippery conditions in Östersund. Using the HHP system reduces the numbers of hours of slippery conditions, due to the deposition of water vapor from the air to the road surface, by 94%, from 2009 h to 128 h.

Table 3-5. Annual required energy for anti-icing and number of hours of slippery conditions on the road surface with and without heating system (Geometry of the HHP system are presented in Table 3-4).

Annual required energy for anti-icing, E_r (kWh/(m^2 · year))	Number of hours that the surface temperature is below 0 ˚C, without heating (h)	Remaining slippery hours, due to the deposition, without heating (h)	Remaining hours of the slippery conditions, due to the deposition, after heating, $t_{slippery}$ (h)
75.3	3440	2009	128

In order to investigate how pre-heating the road surface can influence the anti-icing performance of the HHP system, six different temperature thresholds for pre-heating the road surface are taken into account. The thresholds are: 0°C, 0.1°C, 0.2°C, 0.4°C, 0.8°C and 1.6 °C. The results related to the annual required energy for anti-icing and the remaining slippery hours on the road surface are presented in Figure 3-6.

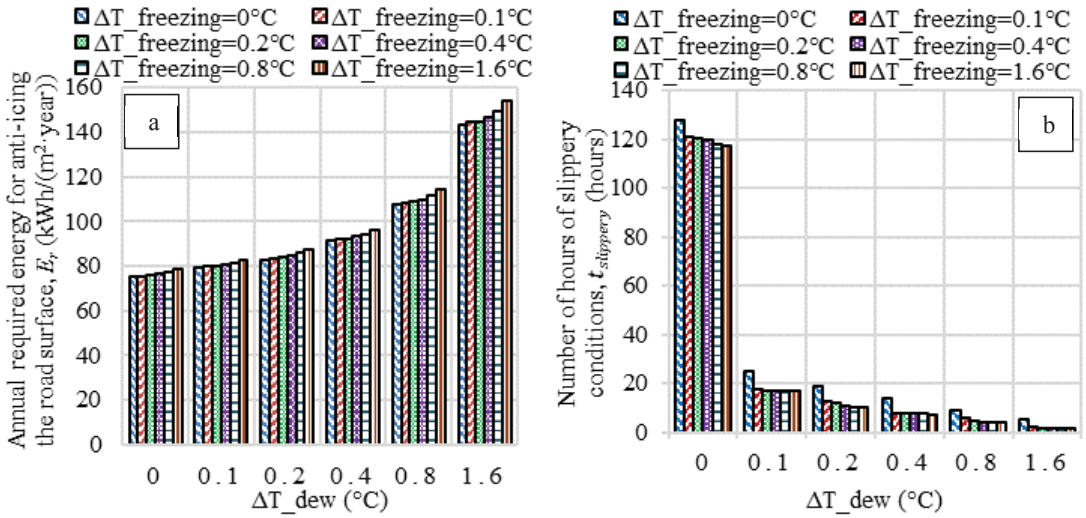

Figure 3-6. The effects of pre-heating on the anti-icing performance of the HHP system (a) the annual required energy (b) the remaining slippery hours on the road surface.

If $E_{r\_initial} = 75.3\ \mathrm{kWh/(m^2 \cdot year)}$ and $t_{slippery\_initial} = 128\ \mathrm{h}$, the relative difference of the remaining hours of slippery conditions to the relative difference of the annual required energy, SR (-), for each specific combination of ΔT_{dew} and $\Delta T_{freezing}$ is as Figure 3-7.

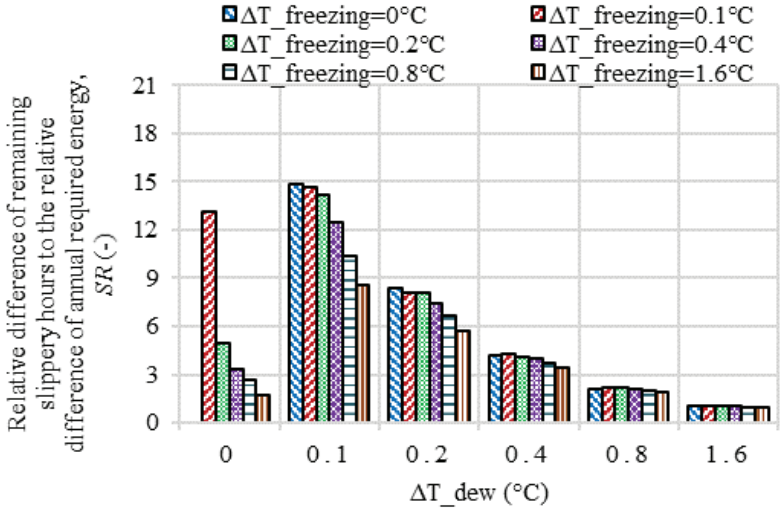

Figure 3-7. Relative difference of remaining hours of slippery condition to the relative difference of annual required energy for different cases of pre-heating.

As can be seen from Figure 3-7, the value of *SR* is more sensitive to variations of ΔT_{dew} compared to that of $\Delta T_{freezing}$. For example, keeping $\Delta T_{freezing} = 0.1$°C constant and varying ΔT_{dew} from 0.1°C to 0.2°C results in a 45% reduction in the *SR*, while keeping $\Delta T_{dew} = 0.1$°C constant and varying $\Delta T_{freezing}$ from 0.1°C to 0.2°C results in only a 3.5% reduction in the *SR*. It is worth mentioning that the sensitivity of *SR* to variations of ΔT_{dew} and $\Delta T_{freezing}$ reduces by increasing their values from 0.1°C to 1.6°C. The minimum value of *SR* is 0.9 which is related to $\Delta T_{dew} = 1.6$°C and $\Delta T_{freezing} = 1.6$°C. In addition, the maximum value of *SR* is 14.8 which is related to $\Delta T_{dew} = 0.1$°C and $\Delta T_{freezing} = 0$°C.

4. Hybrid three dimensional (3D) numerical simulation model

This chapter presents: (i) the development of hybrid 3D numerical simulation model, (ii) the validation of the hybrid 3D model, (iii) the results related to harvesting and anti-icing operations and (iv) the long-term operation of the HHP systems.

4.1. Development of the hybrid 3D numerical simulation model

Figure 4-1 shows a scheme of the hybrid 3D numerical simulation model of the HHP system. As can be seen, the HHP system is divided into a finite number of sub-sections. For each sub-section, the hybrid 3D model of the HHP system is represented by 2D vertical cross sections which are perpendicular to the pipe direction. All 2D vertical cross sections are serially connected to each other through the convective heat transfer in the fluid, circulating along the pipe. The hybrid 3D numerical simulation model simultaneously calculates the transient heat flowing out from the pipes using the finite element method and the temperature decline of the fluid along the pipe using a quasi-steady state assumption.

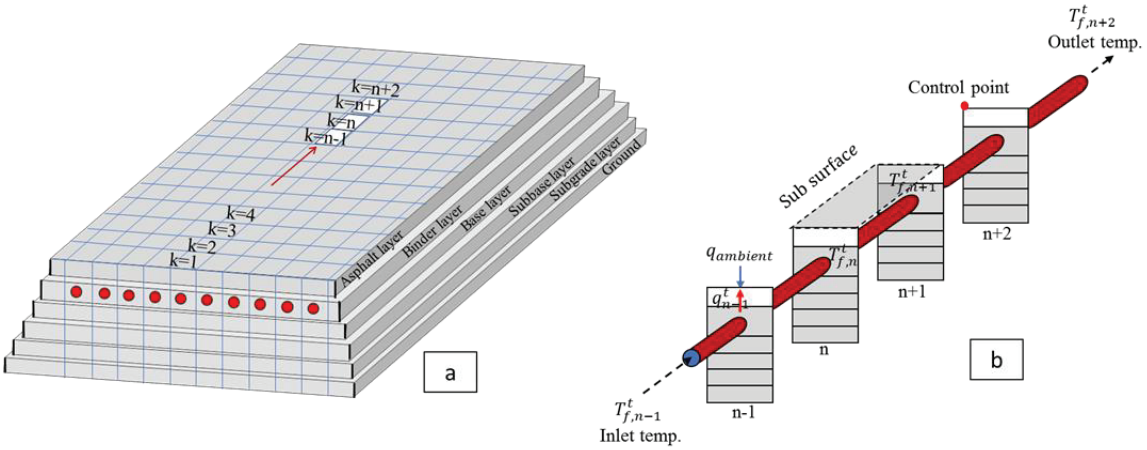

Figure 4-1. A scheme of the hybrid 3D numerical simulation model of a HHP system (a) hybrid 3D model of a HHP system is divided into a finite number of sub-sections (b) the 3D model of the HHP system is represented by 2D vertical sections.

In each 2D vertical cross section, the heat flowing out from the pipes is calculated using an equivalent temperature surrounding the pipe, $T_{eq-pipe}$ (K), and an equivalent thermal resistance between the fluid and the embedded materials, $R_{eq-pipe}$ (m · K/W). $R_{eq-pipe}$ consists of three serially coupled thermal resistances of: (i) the thermal resistance at inner pipe surface, R_{PWS} (m · K/W), (ii) the pipe material resistance, R_p (m · K/W), and (iii) the thermal resistance between the outer pipe wall and an additional annulus, $R_{i,j}$ (m · K/W). Hence, the value of $R_{eq-pipe}$ can be calculated as:

$$R_{eq-pipe} = R_p + R_{i,j} + R_{PWS} \tag{4-1}$$

$$R_p = \frac{\ln(\frac{r_{outer}}{r_{inner}})}{2 \cdot \pi \cdot \lambda_{pipe}} \tag{4-2}$$

$$R_{i,j} = \frac{\ln(\frac{r_{i,j}}{r_{outer}})}{2 \cdot \pi \cdot \lambda_{i,j}} \tag{4-3}$$

$$R_{PWS} = \frac{1}{\pi \cdot \lambda_f \cdot \mathrm{Nu}} \quad \left(\text{where } \mathrm{Nu} = \begin{cases} 4 & \text{if } \mathrm{Re} \leq 2300 \\ 0.023 \cdot \mathrm{Re}^{0.8} \cdot \mathrm{Pr}^{\frac{1}{3}} & \text{if } \mathrm{Re} > 2300 \end{cases}\right) \tag{4-4}$$

where r_{outer} (m) is the outer radius of the pipe, r_{inner} (m) is the inner radius of the pipe, λ_{pipe} (W/(m · K)) is the thermal conductivity of the pipe, $r_{i,j}$ (m) is the radius of the additional annulus surrounding the pipe, $\lambda_{i,j}$ (W/(m · K)) is the thermal conductivity of the surrounding materials, λ_f (W/(m · K)) is the thermal conductivity of fluid, Nu (-) is the Nusselt number, Re (-) is the Reynolds number and Pr (-) is the Prandtl number.

Furthermore, if T_f (K) is the temperature of fluid, circulating through the pipe, and $q_{i,j}$ (W/m^2) is the heat flow between the fluid and the embedding materials, the value of $T_{eq-pipe}$ can be calculated as:

$$T_{eq-pipe} = T_f - q_{i,j} \cdot R_{eq-pipe} \tag{4-5}$$

The longitudinal fluid temperature distribution and the transversal heat transfer process along the pipe are calculated using a steady state solution as:

$$v_f \cdot \pi \cdot {r_{inner}}^2 \cdot \rho_f \cdot c_{p,f} \cdot \frac{\partial T_f(x)}{\partial x} + \frac{T_f(x) - T_{eq-pipe}(x)}{R_{eq-pipe}} = 0 \tag{4-6}$$

where x (m) is the longitudinal length coordinate along the fluid motion, ρ_f (kg/m^3) is the density of fluid, v_f (m/s) is the average velocity of fluid through a cross section of pipe and $c_{p,f}$ (J/(kg · K)) is the specific heat capacity of fluid.

The length of pipe between two 2D vertical cross sections with labels of n and n+1 is L_n. For this section of pipe, the inlet temperature of the fluid at time t is $T_{f,n}^t$ and the outlet temperature is $T_{f,n+1}^t$. Considering the steady state longitudinal fluid temperature distribution along the pipe, the analytical solution to obtain the outlet fluid temperature is calculated as:

$$T_{f,n+1}^t = T_{eq-pipe,n}^t + (T_{f,n}^t - T_{eq-pipe,n}^t) \cdot e^{-(L_n/l_n)} \tag{4-7}$$

where l_n (m) is the characteristic length related to the interaction between the convective heat transfer along the pipe and the transversal heat flow. The value of l_n can be calculated as:

$$l_n = R_{eq-pipe} \cdot v_f \cdot \pi \cdot {r_{inner}}^2 \cdot \rho_f \cdot c_{p,f} \tag{4-8}$$

In this study, the fluid inlet temperature at section 1, $T_{f,1}^{t}$ (K), for each time step is a known value. By applying Equation 4-7, it will be possible obtain the outlet temperature of fluid at the section 1 at time step t. The outlet temperature of section 1 can be used as the inlet temperature of the section 2. Applying this strategy for all sections of pipes; i.e. considering the outlet temperature of one section as the inlet temperature of the next section, will lead to obtain the outlet temperature of last section, $T_{f,\mathrm{n+1}}^{t}$ (K). The value of $T_{f,\mathrm{n+1}}^{t}$ is equal to the outlet temperature of the whole length of the pipe in the HHP system at time t. The details of development hybrid 3D numerical simulation model are provided in Section 3 of **Paper IV.**

Criteria for slippery conditions on the road surface is the same as in Section 3-3 in this thesis. In order to start harvesting solar energy, five different air temperatures of 6 ℃, 8 ℃, 10 ℃, 12 ℃ and 16 ℃ are arbitrary selected. If T_{limit} (℃) is one of the mentioned five temperatures, then the criterion to start harvesting solar energy can be written as:

$$T_{air} > T_{limit} \tag{4-9}$$

Harvesting solar energy will cause a decrease in the temperature of the road surface. The temperature decreases on the road surface during harvesting period, $T_{decrease}$ (℃), can be calculated as:

$$T_{decrease} = T_{unheated} - T_{harv} \tag{4-10}$$

where $T_{unheated}$ (℃) is the surface temperature of an unheated road and T_{harv} (℃) is the surface temperature of the HHP system during harvesting period at the control point, see Figure 4-1.

The annual required energy for anti-icing the road surface using the temperature difference between the inlet and outlet fluids, E_r ($\mathrm{kWh/(m^2 \cdot year)}$), is calculated as:

$$E_r = \frac{\int_{t=0}^{1\ year} (T_{out-r} - T_{in-r}) \cdot v_f \cdot \pi \cdot {r_{inner}}^2 \cdot \rho_f \cdot c_{p,f} \cdot dt}{c_r \cdot L_r} \quad \left(\text{if} \begin{cases} T_{surface} < T_{dew} \\ T_{surface} < T_{freezing} \end{cases}\right) \tag{4-11}$$

Moreover, the annual harvested solar energy, E_h ($\mathrm{kWh/(m^2 \cdot year)}$), can be calculated as:

$$E_h = \frac{\int_{t=0}^{1\ year} (T_{out-r} - T_{in-r}) \cdot v_f \cdot \pi \cdot {r_{inner}}^2 \cdot \rho_f \cdot c_{p,f} \cdot dt}{c_r \cdot L_r} \quad (\text{if } \{T_{air} > T_{limit}) \tag{4-12}$$

where c_r (m) is the distance between pipes in the HHP system, L_r (m) is the pipe length of the HHP system, v_f (m/s) is the velocity of fluid, r_{inner} (m) is the inner radius of the pipe, ρ_f ($\mathrm{kg/m^3}$) is the density of fluid and $c_{p,f}$ ($\mathrm{J/(kg \cdot K)}$) is the specific heat capacity of fluid.

It is important to note that whenever the harvesting or the heating system is turned on, the fluid starts circulating along the HHP system. However, whenever the harvesting or the heating system is turned off, the boundary conditions at the inner surface of the pipe walls of all 2D vertical cross sections are set to be adiabatic.

4.2. Validation of the hybrid 3D numerical simulation model

The hybrid 3D numerical simulation model is validated using: (i) a laboratory experimental test, (ii) an analytical solution, (iii) the results of another numerical simulation model related to a road and (iv) the results of another numerical simulation model related to a bridge.

4.2.1. Validation using the laboratory experimental test

The hybrid 3D numerical simulation model of the HHP system is validated by an laboratory experimental results, obtained from the literature [38]. The HHP system in the experimental test consisted of a one-layer concrete pavement and the embedded pipes. The material of pipe was high-density polyethylene. The dimention of the experimental sample was 1000 mm × 1000 mm × 300 mm (length × width × thickness). The distance between pipes was 200 mm (center to center) and the embedded depth of pipes was 50 mm (from surface to center). A schematic view of the experimental test is shown in Figure 4-2.

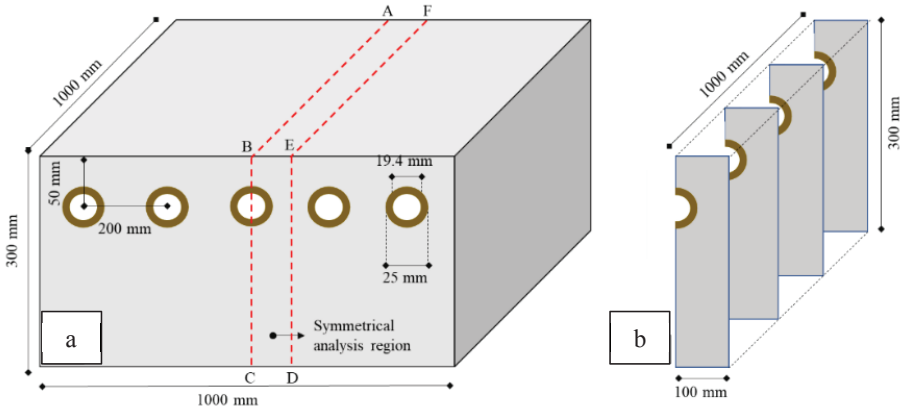

Figure 4-2. The schematic view of hydronic heating pavement (a) a 3D model and (b) a hybrid 3D model used for numerical simulation

The detail related to thermal properties of the materials and the boundary condition are provided in Section 2-2 of **Paper VI**.

From literature [38], the average temperature at the surface between two pipes was given at the time of 120 min. Hence, in order to validate the hybrid 3D numerical simulation model, the heating process was solved for 120 min. The average temperature at the surface along the half distance between pipes at time of 120 min, obtained from the experimental test and the hybrid 3D numerical simulation model, is shown in Figure 4-3. As can be seen, the experimental and numerical simulation results are matching well, so the maximum relative error is 2.4%. It should be noted that the relative error is defined as the difference between the results of the numerical simulation model and experimental test divided to the results of the experimental test.

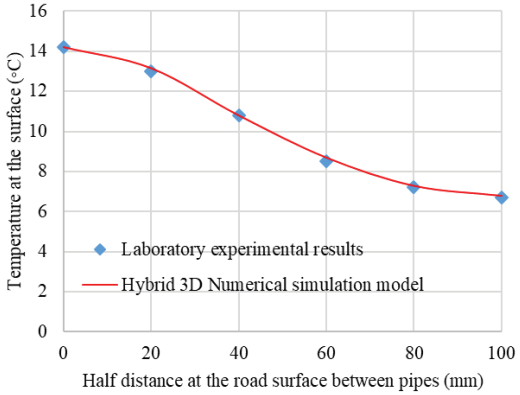

Figure 4-3. Comparison of the results related to the laboratory experimental test [38] and the hybrid 3D numerical simulation model (at the time of 120 min).

4.2.2. Validation using the analytical solution

This section presents the results associated with the fluid temperature variation along the pipe length, calculated by an analytical solution and the numerical simulation model. The analytical solution is based on a steady- state study. The HHP system consists of a one-layer road and a single embedded pipe. The pipe is assumed to be located in the middle of an infinite array of pipes [55]. The ambient temperature is set to be 0 °C and the surface thermal resistance varies from 0 $(m^2 \cdot K)/W$ to 0.1 $(m^2 \cdot K)/W$. Other boundaries are set to be adiabatic. The schematic view of the investigated domain is shown in Figure 4-4.

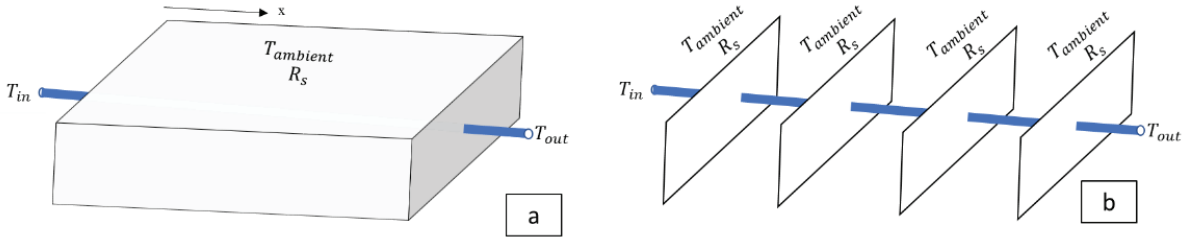

Figure 4-4. Heat extraction with a varying temperature along the pipe (a) analytical solution (b) numerical simulation model ($T_{ambient}$ = 0 °C and R_s = (i) 0 $(m^2 \cdot K)/W$ (ii) 0.05 $(m^2 \cdot K)/W$ (iii) 0.1 $(m^2 \cdot K)/W$).

It is assumed that the road and pipe materials are homogenous. The analytical solution accounts for the distance between the pipes, the embedded depth of the pipes, the pipe diameter, the thermal conductivity of road and pipe materials, the surface thermal resistance, the length of the pipes, the fluid flow rate and the fluid properties (density and specific heat capacity). The length of pipe is set to be L (m) ($0 \leq x \leq L$, see Figure 4-4). The inlet temperature of fluid is T_{in} (K) and the outlet temperature at $x = L$ is T_{out} (K). The equations related to the analytical simulation model as well as the thermal properties of the materials are presented in Section 2 of **Paper V.**

The results associated with the fluid temperature variation along the pipe length are shown in Figure 4-5. As can be seen, the results related to the analytical solution and the numerical simulation are matching well with each other, so the maximum relative error is 2.3% which is related to the case that $R_s = 0$ $(m^2 \cdot K)/W$. The maximum relative error is defined as the difference between the results of analytical solutions and numerical model divided to the results

of the analytical solution. By increasing the surface thermal resistance, the maximum relative error will decrease; e.g., for $R_s = 0.1\ (\mathrm{m}^2 \cdot \mathrm{K})/\mathrm{W}$ the maximum relative error is 2%. It should be noted that an increase in the number of cross-sections will lead to a decrease in the maximum relative error. For example, for the numerical model with eight cross-sections the maximum relative error is 1.4% and for the numerical model with 11 cross-sections the maximum relative error is 0.06%.

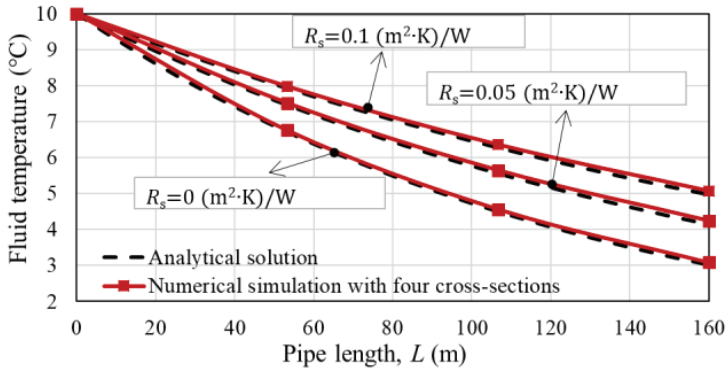

Figure 4-5. Fluid temperature variation along the pipe length considering different surface thermal resistances.

4.2.3. Validation using another numerical simulation model related to a road

In this section, the hybrid 3D numerical simulation model is validated by the results of another numerical simulation study from the literature [40] which was about heat-collecting properties of asphalt pavement as solar collector by a three-dimensional unsteady model. The solar collector consisted of a one-layer asphalt pavement and the embedded pipes. The dimension of the solar collector was 4 m × 4 m × 0.7 cm (length × width × thickness). The pipes were located in a serpentine configuration. The total length of pipe was 63.15 m. The distance between pipes was 0.25 m (center to center) and the embedded depth of pipes was 60 mm (from surface to center). The fluid was set to be water. The velocity of fluid, circulating along the pipes, was 0.3 m/s. The surface boundary was exposed to the solar radiation, convection and longwave radiation. The solar radiation was kept the constant value of 1080 $\mathrm{W/m^2}$. The bottom and side boundaries of the solar collector were set to be adiabatic. For more details, the reader is refered to [40]. The schematic view of the solar collector is shown in Figure 4-6.

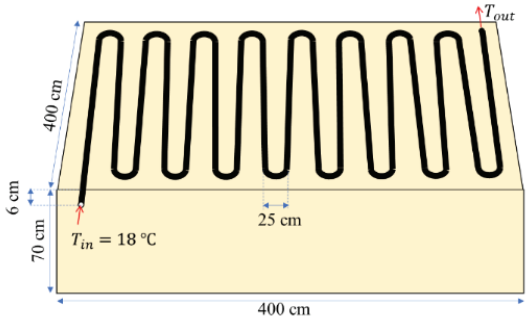

Figure 4-6. A schematic view of the geometry design for the solar collector used to make the numerical simulation model in the literature [40].

The thermal properties of the materials are presented in Section 3-2 of **Paper IV**. The outer and inner diameters of pipe were assumed to be 20 mm and 15 mm. Furthermore, the value of

absorptivity and emissivity were set to 0.85 (-). The valiation were done for two cases:

- Case 1: the ambient air temperature was 25 ˚C and the initial temperature was 20 ˚C.
- Case 2: the ambient air temperature was 34 ˚C and the initial temperature was 30 ˚C.

The validation was done based on: (i) the temperature of aspahlt pavement at the depth of 2.5 cm and (ii) the outlet temperature of fluid. From the literature [40], the temperature variation was given for 120 min. Hence, in order to validate the hybrid 3D numerical simulation model, the harvesting process was run for the same time with the time step of 1 min. The validation results are shown in Figure 4-7.

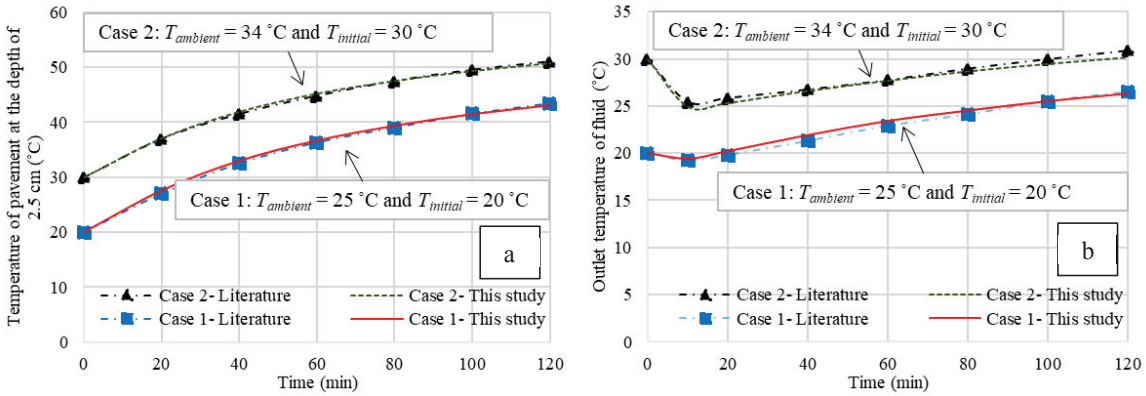

Figure 4-7. Comparing the results obtained from numerical simulation model in the literature [40] and the hybrid 3D numerical simulation models in this study for two different cases (a) the temperature of asphalt pavement at the depth of 2.5 cm and (b) the outlet temperature of fluid.

As can be seen from Figure 4-7 (a), the temperature of the asphalt pavement at the depth of 2.5 cm obtained from the literature [40] and the hybrid 3D numerical simulation models in this study are matching well with together. The absolute temperature difference between the two models for the case 1 is 0.3 ˚C with the standard deviation of 0.2 ˚C and that for case 2 is 0.2 ˚C with a standard deviation of 0.2 ˚C. Furthermore, from Figure 4-7 (b), the outlet temperature of fluid, obtained from the literature [40] and the hybrid 3D numerical simulation models in this study have good match with together, so the absolute temperature difference between the two models for the case 1 is 0.3 ˚C with a standard deviation of 0.2 ˚C and that for case 2 is 0.4 ˚C with a standard deviation of 0.3 ˚C.

4.2.4. Validation using another numerical simulation model related to a bridge

In this section, the hybrid 3D numerical simulation model is validated by the results of another numerical simulation study from the literature [39]. The numerical simulation model from the literature [39] investigated the performance of the HHP system for snow melting of a bridge. The bridge consisted of a one-layer concrete pavement and the embedded pipes. The pipe material was high-density polyethylene. The dimension of the bridge was 9.1 m × 6.1 m × 0.152 m (length × width × thickness). The pipework was in a serpentine configuration, perpendicular to traffic direction on the bridge. The total length of pipe was 198 m. The distance between pipes was 0.305 m (center to center) and the embedded depth of pipes was 89 mm (from surface to center). The outer diameter of pipe was 19 mm and the inner diameter of pipe

was 15 mm. The fluid was 42% propylene glycol-water mixture. The fluid flow rate was 45.6 lit/min. For more details, the reader is refered to [39,56]. The schematic view of the bridge is shown in Figure 4-8. The thermal properties of materials are provided in Section 3-1 of **Paper VII**.

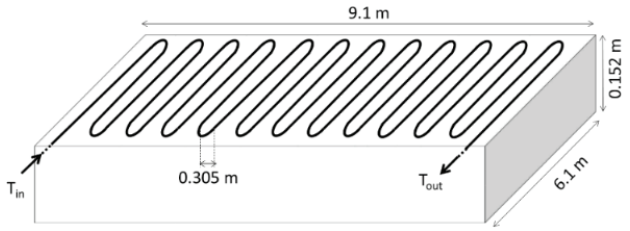

Figure 4-8. A schematic view of the geometry design for the bridge used to make the numerical simulation model in the literature [39].

For validation, the surface boundary of the bridge was set to the calculated temperatures from [56]. Furthermore, the bottom boundary of the bridge was set to the convective heat flux and longwave radiation. The side boundaries of the bridge were assumed to be adiabatic. To validate the hybrid 3D numerical simulation model, the inlet temperature of fluid was used as the input data and the outlet temperature of fluid was used as the output data. The duration of the data was 18340 min with the time interval of 10 min. Hence, the hybrid 3D numerical simulation model was run for the same time duration with a time step of 10 min. The outlet temperature of fluid, calculated by the numerical simulation model from the literature [39] and the hybrid 3D numerical simulation model in this study are presented in Figure 4-9.

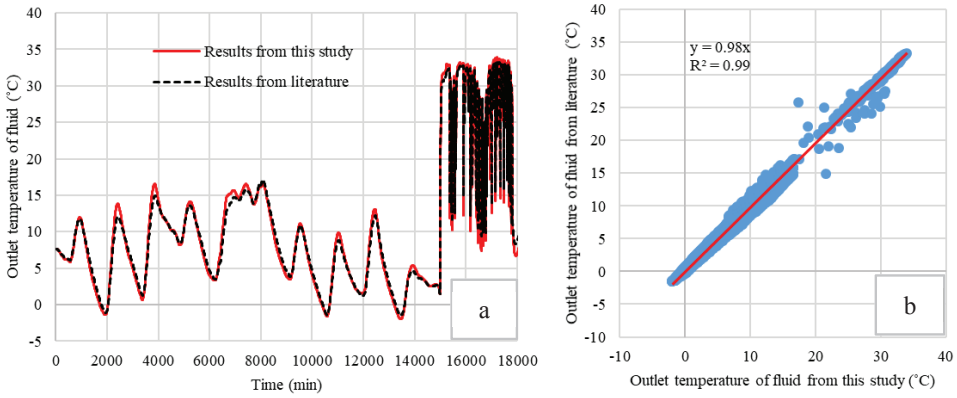

Figure 4-9. Comparing the outlet temperature of fluid obtained from the hybrid 3D numerical simulation models in this study and the model from the literature [39] (a) the outlet temperature of fluid versus time and (b) the scatter plot of the outlet temperature of fluid.

Figure 4-9 (a) illustrates the outlet temperature of the fluid, calculated by the numerical simulation model from the literature [39] and the hybrid 3D numerical simulation model in this study. As can be seen, the results of two numerical simulation models are matching well, so the absolute temperature difference between the two models is 0.6 ˚C with the standard deviation of 0.6 ˚C. Furthermore, Figure 4-9 (b) illustrates the scatter plot of the outlet temperature of fluid, obtained from the hybrid 3D model in this study and the numerical simulation model from the literature [39]. As can be seen, the vertical axis, y (°C), is the outlet temperature of the fluid from the numerical simulation model of the literature [39] and the horizontal axis, x (°C), is the outlet temperature of fluid from the hybrid 3D numerical model in this study. For the best case,

y= x with $R^2 = 1$. Due to some uncertainty in the thermal properties of materials in the literature [39,56], especially the thermal conductivity of the concrete pavement, the relation between x and y in this study is y= 0.98 x with $R^2 = 0.99$.

4.3. Results related to the harvesting and anti-icing operations

In the previous experimental studies [24,29], the fluid temperature varied at a range between 25°C and 50°C. This range of temperature was used to snow melting, however, is high for anti-icing the road surface. In this study, seven fluid temperatures of 4 °C, 6 °C, 8 °C, 10 °C, 12 °C, 16 °C and 20 °C are taken into account to simulate the anti-icing and harvesting operations. The results related to the annual harvested solar energy and the annual required energy for anti-icing the road surface, the average outlet temperatures of the fluid in the HHP system during harvesting and anti-icing periods, the average temperature reduction on the road surface during the harvesting period and the remaining number of hours of the slippery conditions on the road surface during anti-icing period are shown in Figure 4-10.

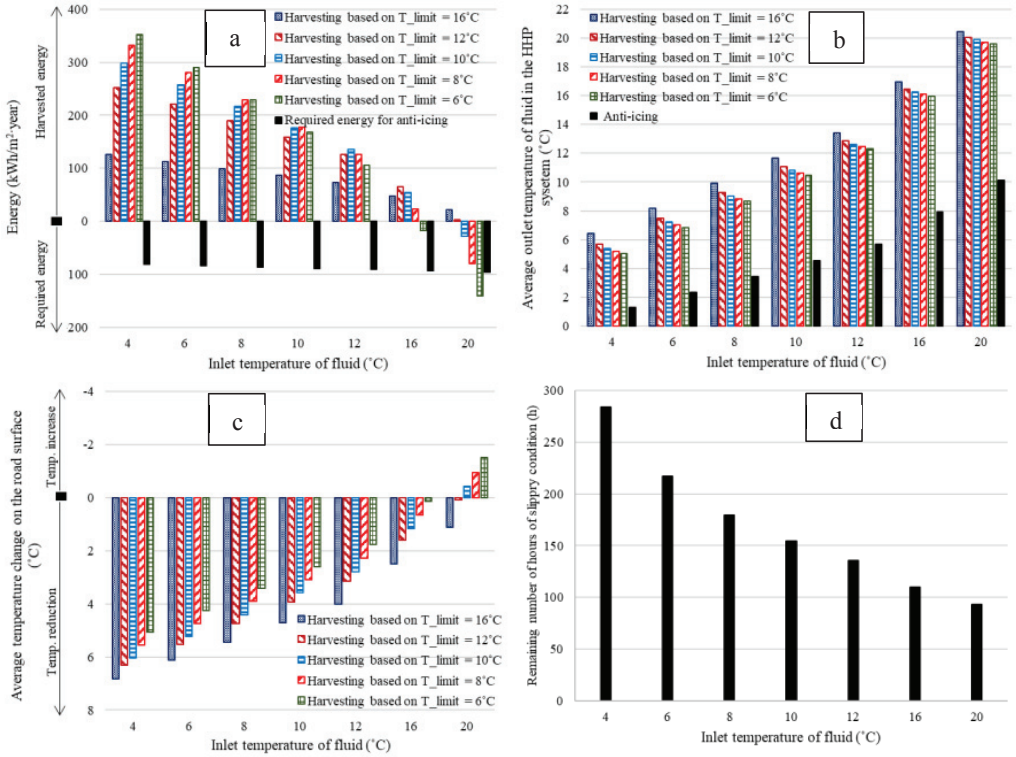

Figure 4-10. The results of (a) the harvested solar energy and the required energy for anti-icing, (b) the average outlet temperatures during the harvesting and the anti-icing periods, (c) the average temperature reduction on the road surface during harvesting period and (d) the remaining number of hours of slippery conditions on the road surface.

The harvested solar energy highly depends on the value of T_{limit}, see Equation 4-9. In order to harvest maximum possible solar energy from the road surface, it is essential to use a suitable combination of T_{in} and T_{limit}. The combinations of 4 °C $\leq T_{in} \leq$ 6 °C and $T_{limit} = 6$ °C, 8 °C $\leq T_{in} \leq 10$ °C and $T_{limit} = 8$ °C, $T_{in} = 12$ °C and $T_{limit} = 10$ °C, $T_{in} = 16$ °C and $T_{limit} = 12$ °C as well as $T_{in} = 20$ °C and $T_{limit} = 16$ °C lead to the maximum values of E_h associated with each inlet fluid temperature. The maximum harvested solar energy during summer is 352.1 kWh/(m^2 · year) which is related to $T_{in} = 4$ °C and $T_{limit} = 6$ °C. It is worth mentioning

that for 4 ℃ $\leq T_{in} \leq$ 12 ℃, the harvested solar energy can be higher than the required energy for anti-icing the road surface. However, for $T_{in} \geq 16$ ℃, the harvested solar energy is always lower than the required energy for anti-icing the road surface. Furthermore, Figure 4-10 (b) illustrates the variation of average outlet temperature of the fluid, T_{out}, versus T_{in}. During both harvesting and anti-icing periods, an increase in T_{in} will results in an increase in T_{out}. During harvesting period by increasing T_{in} from 4 °C to 20 °C, the average value of T_{out} related to all values of T_{limit} increases from 5.6 °C to 19.9 °C. It should be noted that considering a higher value of T_{in} and a lower value of T_{limit} can result in heating the road surface during harvesting period, rather than harvesting solar energy. This results the average value of T_{out} gets lower than T_{in} when $T_{in} = 20$ ℃. Furthermore, during anti-icing period by increasing T_{in} from 4 °C to 20 °C, the value of T_{out} increases from 1.3 °C to 10.2 °C.

Figure 4-10 (c) illustrates the average temperature reduction on the road surface, $T_{decrease}$, at "Control point", see Figure 4-1. By increasing T_{in} from 4 °C to 20 °C, the value of $T_{decrease}$ follows a decreasing trend from 6 °C to – 0.3 °C, on an average value for all T_{limit}. $T_{decrease} <$ 0 ℃, which occurs for $T_{in} = 20$ ℃ and 6 ℃ $\leq T_{limit} \leq 10$ ℃, means that the temperature of the road surface is increasing during harvesting period, rather than decreasing. Furthermore, Figure 4-10 (d) illustrates the number of hours of the slippery conditions on the road surface, $t_{slippery}$. As can be seen, by increasing T_{in} from 4 °C to 20 °C, the value of $t_{slippery}$ reduces down from 284 h to 93 h.

4.4. Long term operation of the HHP system

In this section of the thesis, it is assumed that harvested solar energy during summer is injected to the Borehole Thermal Energy Storage (BTES) and the required energy for anti-icing the road surface during winter is extracted from the BTES. From Figure 4-10, for $T_{in} \leq 12$ ℃, the annual harvested solar energy is higher than the annual required energy for anti-icing the road surface. However, considering the thermal interference between the heat-carrier fluid in the BTES and the undisturbed surrounding ground, the injected heat to the BTES can freely transfer to the surrounding ground [57]. The heat losses from the BTES to the surrounding ground can influence the operation of the BTES on long-term [58]. Hence, in order to understand the long-term operation of the BTES, the temperature evolutions at the borehole walls are examined over a 50-year period using a 3D numerical simulation model.

It should be mentioned that, in this thesis, only a basic concept of using the HHP system and the BTES are investigated and the details related to the design and performance of the heat pumps are not studied. The HHP system and the BTES are decoupled from each other and their performance are investigated separately.

The scheme of the BTES with a single borehole are shown in Figure 4-11. The details related to the Figure 4-11 including the boundary condition, thermal properties of the ground, the equivalent temperature at the ground, T_{eq} (℃), the equivalent heat transfer coefficient, h_{eq} ($\mathrm{W/(m^2 \cdot K)}$) can be found in Section 5 of the **Paper IV**.

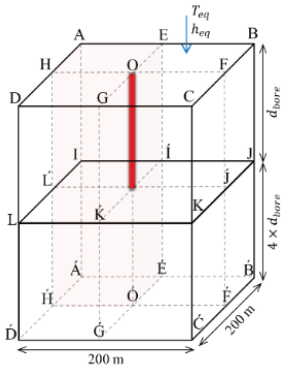

Figure 4-11. A scheme of the BTES including surrounding grounds and boundary conditions.

To obtain the temperature evolution, the conducted heat flux from the pipes to the road surface during the harvesting and anti-icing periods, $q_p(\mathrm{W/m^2})$, is extracted from the hybrid 3D numerical simulation model in Section 4-3 of this thesis. The heat flux of q_p has hourly values in line with the climate data and includes: the harvesting and anti-icing periods as well as the period during which the harvesting/anti-icing is off, $q_p = 0\ \mathrm{W/m^2}$. The hourly heat fluxes during harvesting and anti-icing periods for different inlet temperatures, corresponding to the maximum harvested solar energy in Section 4-3, are shown in Figure 4-12.

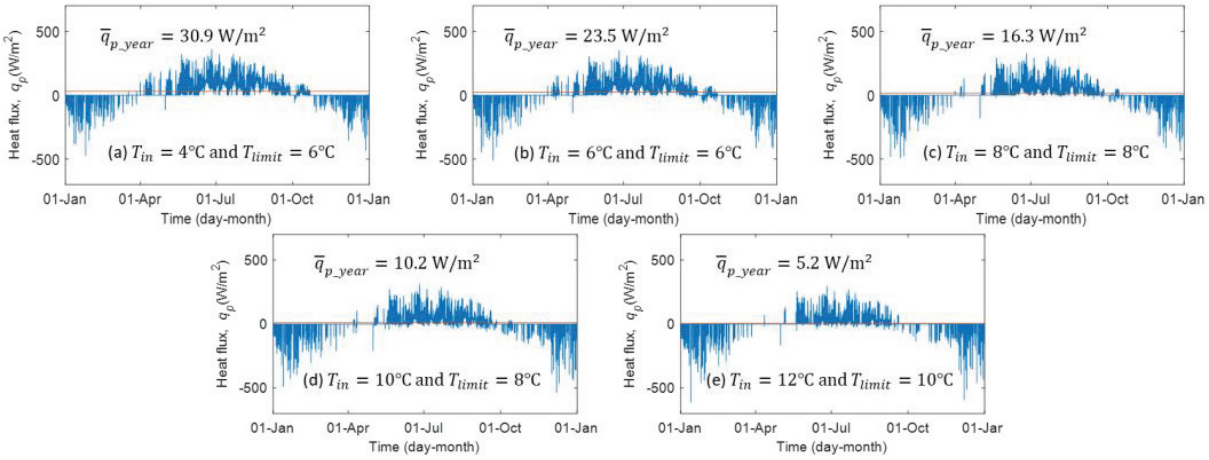

Figure 4-12. Heat fluxes during the harvesting and anti-icing periods for different inlet temperatures of the fluid.

In this thesis, it is assumed that the harvesting process is done using passive heat exchange. Hence, the amount of heat injected to the BTES is considered to be equal to the amount of the heat harvested from the HHP system. However, it is assumed that the anti-icing process is done using heat pump to ensure the required inlet temperature to the HHP system. The injected/extracted heat rate for each borehole, $q_s(\mathrm{W/m})$, can be obtained using the harvested/anti-icing heat fluxes as:

$$q_s = \frac{W_r \cdot L_r}{N \times d_{bore}} \cdot q_p \times f \quad \left(\begin{cases} f = 1 \text{ during harvesting} \\ f = H_f \text{ during anti} - \text{icing} \end{cases} \right) \tag{4-13}$$

$$H_f = \frac{\mathrm{COP_h} - 1}{\mathrm{COP_h}} \tag{4-14}$$

where L_r (m) is the length of the HHP system, W_r (m) is the width of the HHP system, d_{bore} (m) is the depth of one borehole and N is the number of boreholes. In this study, $L_r = 50$ m, $W_r = 3.5$ m and $d_{bore} = 200$ m and N = 20. Furthermore, $\mathrm{COP_h}$ is the coefficient of performance of the heat pump during anti-icing period and H_f is the heat flux adjustment factor for anti-icing. In this thesis, for simplicity of the simulation, three constant $\mathrm{COP_h}$s of 3, 4 and 5 are used [59]. For more details, the reader is referred to Section 5 of the **Paper IV**.

It is assumed that the boreholes are located far from each other and there is no thermal interaction among them, so the total heat loads of the BTES are equally divided among all boreholes.

The results of the average temperature evolution at the borehole walls over 50-year period associated with different inlet temperatures of the fluid in the HHP system and three different $\mathrm{COP_h}$ are presented in Table 4-1. The results are: the inlet temperature of the fluid, T_{in} (°C), the temperature for turning on the harvesting operation, T_{limit} (°C), the annual average heat rate injected/extracted to or from a single borehole, $\overline{q}_{s-year}$ (W/m), the annual spatial average temperature at the borehole walls during 50 years, T_{ave} (°C), the annual amplitude temperature at the borehole walls, T_{amp} (°C) $= (T_{max}$ (°C) $- T_{min}$ (°C))/2, and the annual average temperature change at the borehole wall from the first year to 50th year, T_{change} (°C).

Table 4-1. The results related to the temperature evolution at the borehole walls over 50-year period for different inlet temperatures of the HHP system and three different $\mathrm{COP_h}$s.

T_{in} (°C)	T_{limit} (°C)	$\mathrm{COP_h}$=3				$\mathrm{COP_h}$=4				$\mathrm{COP_h}$=5			
		$\overline{q}_{s-year}$ (W/m)	T_{ave} (°C)	T_{amp} (°C)	T_{change} (°C)	$\overline{q}_{s-year}$ (W/m)	T_{ave} (°C)	T_{amp} (°C)	T_{change} (°C)	$\overline{q}_{s-year}$ (W/m)	T_{ave} (°C)	T_{amp} (°C)	T_{change} (°C)
4	6	1.5	4.9	2.1	0.5	1.5	4.9	2.1	0.5	1.4	4.9	2.1	0.5
6	6	1.2	4.8	2.0	0.4	1.1	4.8	2.1	0.4	1.1	4.8	2.1	0.4
8	8	0.9	4.7	1.9	0.3	0.8	4.7	2.0	0.3	0.8	4.7	2.0	0.3
10	8	0.6	4.6	1.9	0.2	0.6	4.6	1.9	0.2	0.5	4.6	2.0	0.2
12	10	0.4	4.5	1.8	0.1	0.3	4.5	1.9	0.1	0.3	4.5	1.9	0.1

Moreover, Figure 4-13 illustrates the hourly variation of the spatial average temperature evolution at the borehole walls over 50-year period associated with $T_{in} = 6$ °C and $T_{limit} = 6$ °C and $\mathrm{COP_h} = 4$.

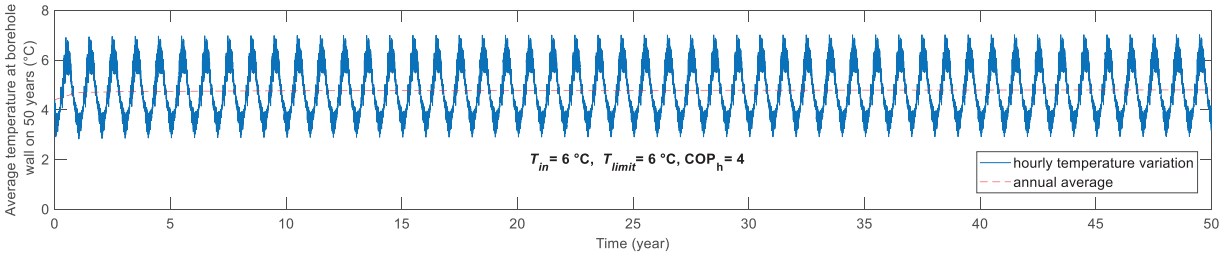

Figure 4-13. Hourly temperature evolution at the borehole walls over 50-year period for $T_{in} = 6$ °C and $T_{limit} = 6$ °C.

As can be seen from Table 4-1, the annual average temperature change at the borehole walls over time is above 0 °C. Furthermore, as can be seen from Figure 4-13, the temperature evaluation over time follows an increasing trend. The temperature increase is significant for the first two years and then slowly trends towards zero with time. The temperature increase at the

borehole walls indicates that the annual heat injected into the ground during harvesting period is higher than the sum of the annual heat extracted from the ground during anti-icing period and the heat losses from the BTES to the surrounding ground. This means that the BTES with 20 borehole and 200 m depth for T_{in} varies between 4 ℃ and 12 ℃ and $\mathrm{COP_h}$ between 3 and 5 can operate reliably over 50 years of operation with a slight improvement comparing to the first year.

.

5. Minimum required energy for anti-icing

This chapter presents: (i) superposition principle for separation of the numerical simulation model of the HHP system into two sub-models, (ii) elementary temperature response (iii) results of the minimum required energy for anti-icing the road surface and (iv) full simulation model of the HHP system using the calculated minimum heat fluxes.

5.1. Superposition principle for the separation of the HHP model

A superposition principle is mathematically based on the linear equation system [52]. The superposition principle can be used if the heat transfer process on the road surface and the thermal properties of materials are independent of the temperature level. The superposition principle is used to separate the numerical simulation model of the HHP system into two fundamental sub-models, namely: (i) a model with supplying heat to the HHP system and (ii) a model without any heat supply. The first sub-model is used to obtain an elementary temperature response and the second sub-model is used to obtain the temperature at the surface of an unheated road. The separation of the numerical simulation model of the HHP system into two sub-models is illustrated in Figure 5-1. As can be seen, the surface boundary of the road is exposed to a constant equivalent heat transfer coefficient, $h_{eq}(\mathrm{W/(m^2 \cdot K)})$, and an equivalent temperature, $T_{eq}(\mathrm{K})$. In Figure 5-1 (b), as the first sub-model, the surface, bottom and initial temperatures of the road are set to be 0°C. In addition, the fluid flow rate is set to be constant. In Figure 5-1 (c), as the second sub-model, the bottom and initial temperatures are set to have the same temperatures as the main numerical simulation model, see Figure 5-1 (a).

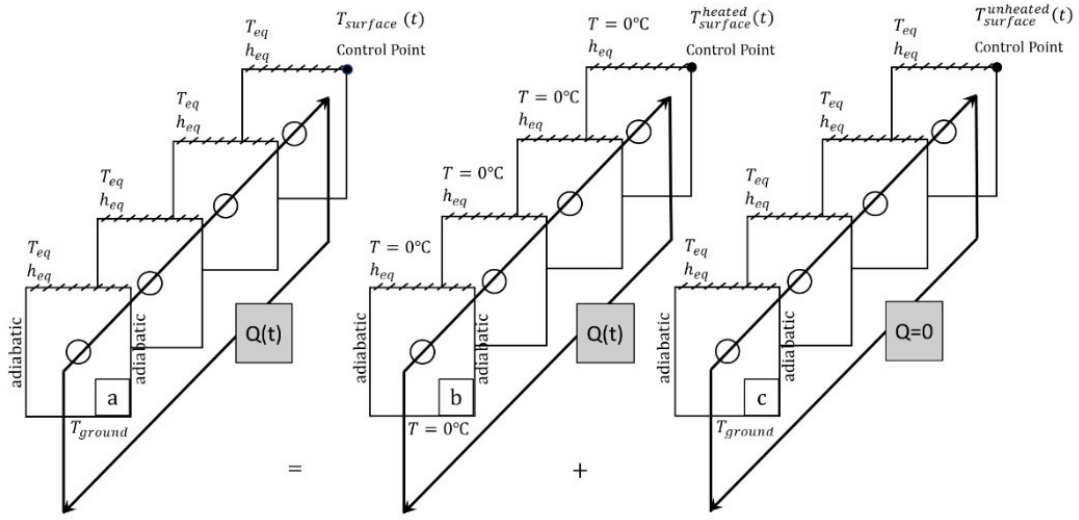

Figure 5-1. Separation of the hydronic heating pavement model into two sub-models using the superposition principle (a) the boundary condition on the road surface consists of the equivalent temperature and the equivalent heat transfer coefficient (b) the sub-model with supplying heat perturbation and (c) the sub-model without supplying any heat.

It is important to note that in this study the variation of the temperature on the road surface is calculated at a point which is located in the middle between two pipes on the surface of the outlet section. This point is called the control point, see Figure 5-1. The temperature variation at the control point, $T_{surface}(t)$ (K), can be obtained by summing the temperature variation at

the control point of the heated road, $T_{surface}^{heated}(t)$ (K), and that at the control point of the unheated road, $T_{surface}^{unheated}(t)$ (K), as:

$$T_{surface}(t) = T_{surface}^{heated}(t) + T_{surface}^{unheated}(t) \quad (5\text{-}1)$$

The value of $T_{surface}^{heated}(t)$ is determined based on the value of the supplied heat to the HHP system, $Q(t)$(W). Furthermore, the value of $Q(t)$ is determined based on the value of $T_{surface}^{unheated}(t)$. It is worth noting that the value of $Q(t)$ is independent of the value of $T_{surface}^{heated}(t)$. In other words, there is no temperature feedback from the road surface to the control system in order to change the value of $Q(t)$. Considering any temperature feedback in the control system will destroy the linear equation assumption and then the principle of superposition.

5.2. Elementary temperature response due to the unit step-change in the heat supply

The elementary temperature response is calculated using the hybrid 3D numerical simulation model of the HHP system. In order to calculate the elementary temperature response, the boundary condition of the road surface is exposed to the equivalent temperature and the equivalent heat transfer coefficient, see Figure 5-1 (b). Furthermore, the heat supply, $Q(t)$, is set to follow Heaviside's unit step-change function, $H(t)$. The Equation of $H(t)$ is as [60]:

$$H(t) = \begin{cases} 1 & t > 0 \\ 0 & t \leq 0 \end{cases} \quad (5\text{-}2)$$

Figure 5-2 (a) shows the variation of the elementary temperature response, u_q (°C/W), induced by a unit step-change in the heat supply. The value of u_q corresponds to the variation of temperature at the control point, see Figure 5-1. The numerical simulation model is run for two-weeks (336 hours). For further time after two weeks, it is assumed that the temperature variation reaches steady-state. To improve the precision of the result, the time step of the simulation is set to be 1 minute. Figure 5-2 (b) shows the results of u_q for the first 30 minutes of the simulation. As can be seen, it takes a few minutes that the supplied heat conducts from the embedded pipes to reach the road surface. Altogether, the variation of u_q versus time consists of three parts: (i) an approximately five minutes initial delay, (ii) a sharp increase for when $t <$ 50 h and (iii) a gradual increase until the value of u_q becomes constant at $t =$ 336 h.

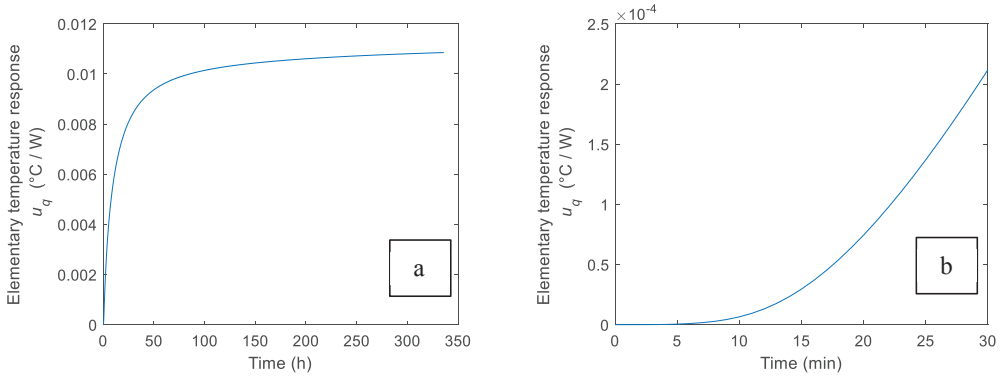

Figure 5-2. Elementary temperature response induced by a step change in the supplied heat (a) the results associated with two weeks simulation and (b) the results associate with the first 30 minutes of the simulation.

The supplied heat to the HHP system, $Q(t)$, is set to follow a step-wise function. As shown in Figure 5-3, the supplied heat is composed by a sequence of heat pulses. The magnitude of heat pulses is set to be 1 W. The length of each heat pulse is t_p (s). The value of t_p is set to be 60 minutes in line with the climate data intervals.

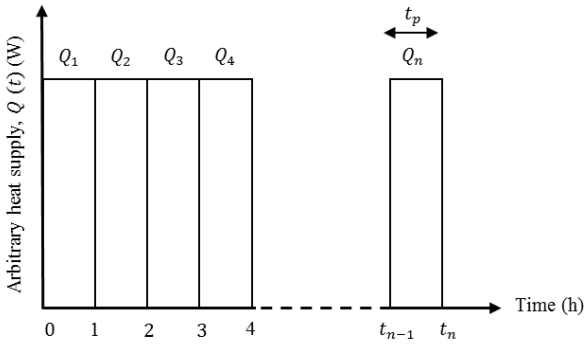

Figure 5-3. The continuous heat supply, $Q(t)$, which is composed by a sequence of heat pulses with the length of t_p.

The temperature response corresponding to a single heat pulse, u_{TSP} (℃/W), can be obtained by assembling two sequences of the elementary temperature responses, u_q (℃/W). The value of u_{TSP}, induced by the heat pulse of Q_n (W), can be obtained by assembling the elementary temperature responses at $t_{n-1} = t_p \cdot (n-1)$ and $t_n = t_p \cdot n$ as:

$$u_{TSP}\,(t_n) = \begin{cases} u_q\left(t - t_p \cdot (n-1)\right) - u_q\left(t - t_p \cdot n\right) & t_p > 0\,,\ n > 0 \\ 0 & \text{else} \end{cases} \qquad (5\text{-}3)$$

Figure 5-4 (a) illustrates the assembling of two sequences of u_T associated with Q_{101} (W), the heat pulse between 100 h and 101 h. Furthermore, Figure 5-4 (b) illustrates the temperature response corresponding to the heat pulse of Q_{101}. As can be seen, there is a delay in the temperature response to reach the maximum value. The delay is due to the time takes for the heat to conduct from the embedded pipes to the road surface. The maximum value of u_{TSP} is 0.0011 ℃/W which occurs 94 minutes after beginning of the heat pulse. The maximum value is located between $1 \times t_p$ and $2 \times t_p$.

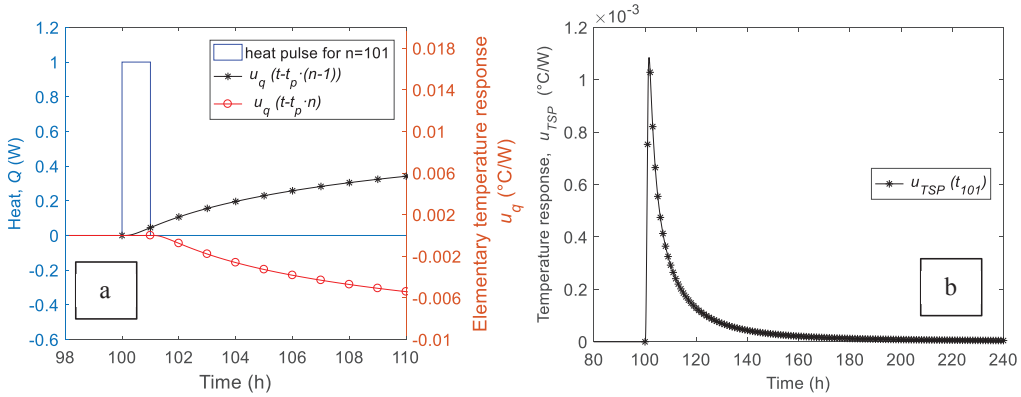

Figure 5-4. The temperature response corresponding to Q_{101}, the heat pulse between 100 h and 101 h (a) the heat pulse and the elementary temperature responses at the time range from 98 h to 110 h and (b) the temperature response for the time range from 80 h to 240 h.

5.3. Calculation of the minimum required energy for anti-icing the road surface

In order to calculate the optimal required energy, it is necessary to calculate the required temperature increase on the road surface for anti-icing the road surface. The required temperature increases, T^+ (℃), can be obtained as:

$$T^+ = \begin{cases} T_{dew} - T_{surface}^{unheated} + T_{threshold} & \text{if } \begin{cases} T_{surface}^{unheated} < T_{dew} \\ T_{surface}^{unheated} < T_{freezing} \end{cases} \\ 0\ ℃ & \text{else} \end{cases} \quad (5\text{-}4)$$

where T_{dew} (℃) is the dew-point temperature and $T_{surface}^{unheated}$ (℃) is the unheated surface temperature when no heat is injected to the HHP system, see Figure 5-1 (c). Moreover, $T_{threshold}$ (℃) is a threshold temperature to ensure that the temperature increase on the road surface will keep the road surface ice-free. It should be noted that $T_{threshold} \geq 0$ ℃ and $T^+ \geq 0$ ℃. The minimum value of T^+ is obtained if $T_{threshold} = 0$℃. Furthermore, the statement of $T^+ > 0$ ℃ is true if the supplied heat to the HHP system is already conducted to the road surface, otherwise $T^+ = 0$ ℃.

As it is presented in Equation 5-5, the temperature increase on the road surface can be obtained by multiplying the temperature response, corresponding to each heat pulse, by the magnitude of the heat pulse. The temperature increase on the road surface is desired to be equal to or more than T^+.

$$A \times Q \geq T^+ \quad (5\text{-}5)$$

$$A = \begin{bmatrix} u_{TSP}^1(t_1) & 0 & \cdots & \cdots & 0 \\ \vdots & \ddots & 0 & \vdots & \vdots \\ u_{TSP}^i(t_1) & \vdots & \ddots & 0 & \vdots \\ \vdots & \vdots & \vdots & \ddots & \vdots \\ u_{TSP}^{n \cdot t_p}(t_1) & \cdots & u_{TSP}^{n \cdot t_p}(t_m) & \cdots & u_{TSP}^{n \cdot t_p}(t_n) \end{bmatrix}_{n \cdot t_p \times n} \quad Q = \begin{bmatrix} Q_1 \\ \vdots \\ Q_i \\ \vdots \\ Q_n \end{bmatrix}_n \quad T^+ = \begin{bmatrix} T_1^+ \\ \vdots \\ T_i^+ \\ \vdots \\ T_{n \cdot t_p}^+ \end{bmatrix}_{n \cdot t_p \times 1}$$

In the above equation, A is a matrix of the temperature responses associated with all sequences of the heat pulses. The matrix of A is a triangular matrix with $n \cdot t_p$ rows and n columns. Considering a constant value for t_p, the values in A only depends on the geometry and the properties of the HHP system. $u_{TSP}^i(t_n)$ is the momentary value of the temperature response corresponding to Q_n at $t = i \cdot t_p$. Furthermore, T_i^+ is the required temperature increase at $t = i$.

Equation 5-5 can be exactly solved for $A \times Q = T^+$. However, the results of the solution include some negative elements in Q. It understood that negative elements in Q means cooling the road surface and positive elements means heating the road surface. Since, in this study, the HHP system is simulated only for heating the road surface, so the values of all elements have to be equal to or more than 0 W, $Q_i \geq 0$ W.

Furthermore, the annual required energy for anti-icing the road surface, E_r (kWh/(m^2 · year), is calculated as:

$$E_r = \int_{i=1}^{1\ year} q_i \cdot dt \quad \text{where} \quad q_i = \frac{Q_i}{c \cdot L} \tag{5-6}$$

where q_i ($\mathrm{W/m^2}$) is the heat flux supplied to the HHP system at time i, c (m) is the distance between the pipes and L (m) is the pipe length. In this chapter, $c = 100$ mm and $L = 50$ m.

By considering q_{max} ($\mathrm{W/m^2}$) as the maximum possible heat flux which can be supplied to the HHP system and E_r as the objective function of the optimization, the optimal required energy for anti-icing the road surface will be calculated as:

$$\min E_r \text{ such that } \begin{cases} A \times Q \geq T^+ \\ 0\ \mathrm{W/m^2} \leq Q/(c \cdot L) \leq q_{max} \end{cases} \tag{5-7}$$

A linear programming optimization was used to solve Equation 5-7. The function was solved using Gurobi Optimizer 7.5 [35], interfaced MATLAB R2016.b environment. The program was run in a computer with 64 GB RAM and a processor of Intel (R) Core (TM) i7-6900K CPU @ 3.2GHz. It is worth noting that Gurobi Optimizer solved Equation 5-7 in less than five minutes, while, solving the same problem using MATLAB Optimization toolbox required much longer time (the solver was still busy after 7 hours without any solution).

The calculated optimal heat flux supplied to the HHP system, $q_{optimal}$ ($\mathrm{W/m^2}$), can be used to obtain the surface temperature of the heated road. The analytical solution to obtain the surface temperature, $T_{surface}^{analytical}$ (°C), can be written as:

$$T_{surface}^{analytical} = A \times Q_{optimal} + T_{surface}^{unheated} \text{ where } Q_{optimal} = q_{optimal} \times c \times L \tag{5-8}$$

By considering $T_{threshold} = 0.49$°C (see Section 8-2 of **Paper VI**) and setting $q_{max} = 200\ \mathrm{W/m^2}$, the optimization results associated with the optimal heat fluxes supplied to the HHP system and the variation of the surface temperature during January will be as Figure 5-5. As can be seen in Figure 5-5 (a), all the heat fluxes are above 0 $\mathrm{W/m^2}$. The maximum heat flux during January is less than 200 $\mathrm{W/m^2}$. Furthermore, the variation of $T_{surface}^{analytical}$ and T_{dew} are illustrated in Figure 5-5 (b). As shown, for when $T_{surface}^{analytical} < 0$°C, the value of $T_{surface}^{analytical}$ is equal to or more than the value of T_{dew}.

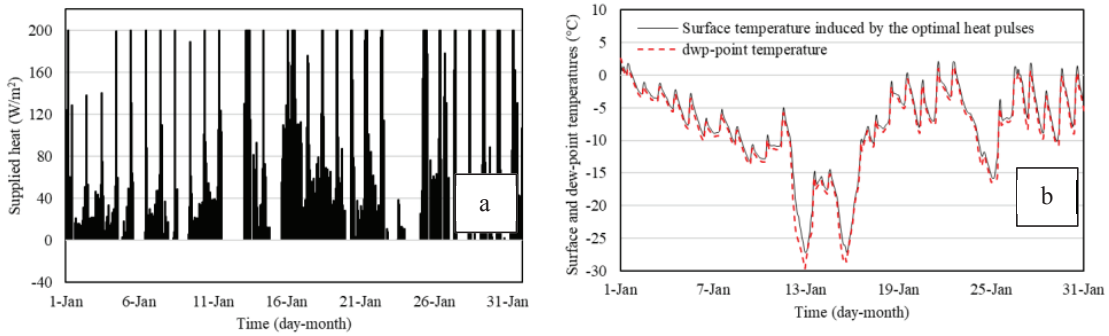

Figure 5-5. Optimization results associated with anti-icing the road surface during January (a) the optimal heat fluxes supplied to the HHP system (b) the surface and dew-point temperatures.

5.4. Full simulation model of the HHP system using the calculated minimum heat fluxes

Figure 5-6 illustrates the process of importing the calculated optimal heat fluxes from the model (a), at which the road surface is exposed to the simplified boundary conditions using T_{eq} and h_{eq}, to the model (b), at which the road surface is exposed to the all heat fluxes of Equations of Table 3-1; i.e. the full simulation model is run.

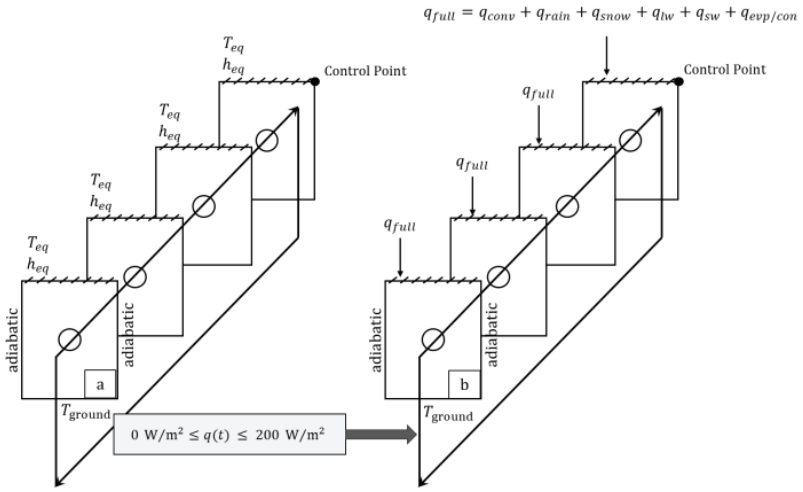

Figure 5-6. Calculation of optimal heat flux supplied to the HHP system for keeping the road surface ice-free at the control point (a) considering a simplified simulation model and (b) considering the full simulation model.

Table 5-1 presents the maximum and mean heat fluxes supplied to the HHP system for a year and different months, the number of hours during which the heating system is turned on, the required energy for anti-icing, the remaining number of hours of the slippery conditions as well as the maximum inlet and outlet temperatures for when the heating system in turned on.

Table 5-1. Maximum and mean heat fluxes supplied to the HHP system, required energy for anti-icing, temperature difference on the road surface between the analytical calculation and the numerical simulation as well as the maximum inlet/outlet temperatures of fluid (the surface is exposed to the all heat fluxes of equations of Table 3-1; i.e. a full simulation model is run). (Standard deviation is related to mean equivalent temperature)

Time	Max. heat flux when the heating system is on (W/m²)	Mean heat flux when the heating system is on (W/m²)	Number of hours during which the heating system is on (h)	Optimal required energy (kWh/m²)	$t_{slippery}^{simulation}$ (h)	Max. T_{in} (℃)	Max. T_{out} (℃)
Year	200	71.59	1489	106.60	3	11.96	10.06
Jan.	200	68.86	454	31.26	2	7.57	5.67
Feb.	200	65.15	298	19.41	0	7.25	5.35
Mar.	173.39	54.40	56	3.05	0	4.11	2.52
Apr.	200	136.03	5	0.68	0	8.63	6.73
May	-	-	0	0.00	0	-	-
June	-	-	0	0.00	0	-	-
July	-	-	0	0.00	0	-	-
Aug.	-	-	0	0.00	0	-	-
Sept.	-	-	0	0.00	0	-	-
Oct.	172.88	54.64	30	1.64	1	6.26	4.62
Nov.	200	55.09	226	12.45	0	7.28	5.64
Dec.	200	90.73	420	38.10	0	11.96	10.06

As can be seen from Table 5-1, considering $q_{max} = 200\ \mathrm{W/m^2}$ for calculation of the optimal heat fluxes supplied to the HHP system results in the maximum inlet temperature of 11.96 °C and the maximum outlet temperature of 10.06°C. From Table 5-1, the annual mean heat flux for when the heating system is turned on is 71.59 $\mathrm{W/m^2}$. The maximum mean heat flux is 136.03 $\mathrm{W/m^2}$ which occurs during April for when the heating system is turned on only for 3 hours. This short period of heating produces $0.68\ \mathrm{kWh/(m^2 \cdot month)}$ energy, which is the minimum value for the required energy. The total number of hours during which the heating system is turned on is 1489 hours. This time of heating produces 106.6 $\mathrm{kWh/(m^2 \cdot year)}$ energy which leads to remaining only 3 hours of the slippery condition on the road surface. Even for these 3 hours, the mean difference between the surface temperature and the dew-point temperature is 0.05 °C with the standard division of 0.02 °C.

6. Coupled HHP system to a Horizontal Ground Heat Exchanger (HGHE)

This chapter presents: (i) the model development of the coupled HHP system to the HGHE, (ii) the results associated with the harvesting solar energy and anti-icing the road surface (iii) the heat loss flowing out from the HGHE to surrounding soil and (iv) the effects of the thermal properties of the ground materials on the efficiency of coupled HHP system to the HGHE for harvesting solar energy and anti-icing the road surface.

6.1. Model development

A hybrid 3D numerical simulation model is used to examine the feasibility of the coupled HHP system to the HGHE for harvesting solar energy during summer and anti-icing the road surface during winter. The details and equations for developing the hybrid 3D numerical simulation model of the coupled HHP system to the HGHE are presented in Section 3-1 of **Paper VII**. A scheme of the coupled HHP system to the HGHE is shown in Figure 6-1.

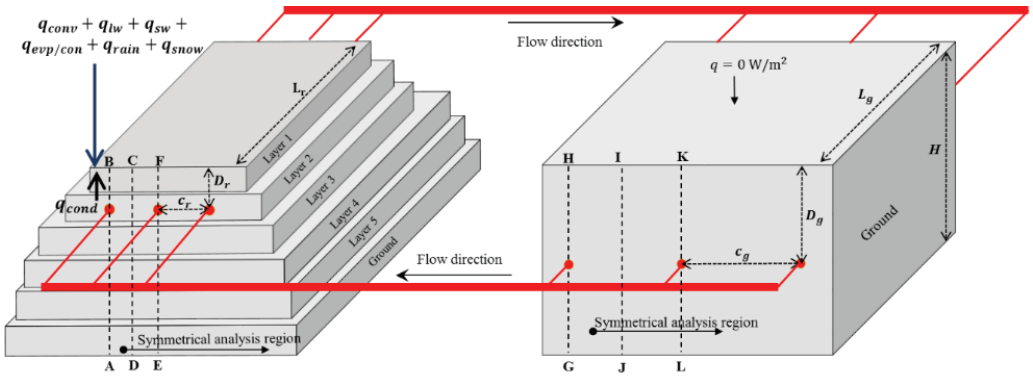

Figure 6-1. Schematic view of the hydronic heating pavement system coupled to the horizontal ground heat exchanger.

The mass and heat balances at the surface of the HHP system are based on Equation 3-1 and Table 3-1. Moreover, the boundary condition at the surface of the HGHE is considered to be adiabatic, by assuming a well insulation layer at the surface of the HGHE. The total depth of the HHP system and the HGHE is truncated to five times of the periodic penetration depth, d_p(m) of the ground soil, see the depth of H in Figure 6-1. The value of H (m) is calculated as:

$$H = 5 \times d_p(\mathrm{m}) = 5 \times \sqrt{\frac{a \times t_p}{\pi}} \qquad (6\text{-}1)$$

where a (m^2/s) is the thermal diffusivity of the ground soil and t_p (s) is the time period. In this study, t_p (s) is considered to be one year. The boundary condition of the ground at the depth of H is set to be adiabatic. In this study, T_{in-r} (°C) is the inlet temperature of fluid in the HHP system, T_{out-r} (°C) is the outlet temperature of the fluid in the HHP system, T_{in-g} (°C) is the inlet temperature of fluid in the HGHE and T_{out-g} (°C) is the outlet temperature of the fluid in the HGHE. It is assumed that $T_{in-r} = T_{out-g}$ and $T_{out-r} = T_{in-g}$.

A close loop piping network is used for coupling the HHP system to the HGHE. The materials, thickness and diameter of embedded pipes in the HHP system and the HGHE are considered to be the same. The pipe material is made of polyethylene (PEX), the thickness of

the pipe is 2.3 mm and the pipe outer diameter is 25 mm. For more details, the reader is referred to Section 3-2 of **Paper VII**.

Criteria for slippery conditions on the road surface is the same as in Section 3-3 in this thesis. Moreover, harvesting solar energy starts when the air temperature is above 10 ˚C. In order to guarantee that the temperature of the fluid, circulating in the HGHE, will not cause a temperature drop in the domain of the HGHE during the harvesting period, it is assumed that the harvesting solar energy starts only if the inlet temperature of the fluid in the HGHE, T_{in-g} (℃), is higher than the average temperature of inner surface of the pipe walls in the HGHE, T_{ave-g} (℃). The mentioned criteria to start harvesting solar energy can be written as:

$$\begin{cases} T_{air} > 10℃ \\ T_{in\_g} > T_{ave\_g} \end{cases} \quad (6\text{-}2)$$

Furthermore, the temperature decreases on the road surface during harvesting period as well as the annual required energy for anti-icing the road surface can be obtained by Equations 4-10 and 4-11, respectively. Moreover, similar to Section 4-1 of this thesis, the annual harvested solar energy, E_h ($\mathrm{kWh/(m^2 \cdot year)}$), can be calculated as:

$$E_h = \frac{\int_{t=0}^{1\ year} (T_{out-r} - T_{in-r}) \cdot v_f \cdot \pi \cdot {r_{inner}}^2 \cdot \rho_f \cdot c_{p,f} \cdot dt}{c_r \cdot L_r} \left(\text{if} \begin{cases} T_{air} > 10\ ℃ \\ T_{in-g} > T_{ave-g} \end{cases} \right) \quad (6\text{-}3)$$

6.2. Feasibility of the coupled HHP system to the HGHE

Figure 6-2 shows the results of the numerical simulation model of the coupled HHP system to the HGHE. The results are: (a) the harvested solar energy and the required energy for anti-icing the road surface, (b) the average temperature of the domains of the HHP system and the HGEH, (c) the remaining number of hours of the slippery conditions on the road surface during heating period, (d) the temperature reduction on the road surface during the harvesting period as well as (e) the inlet and outlet temperatures of fluid, circulating along the HHP system, during harvesting and heating periods. It is important to remind that $T_{in-r} = T_{out-g}$ and $T_{out-r} = T_{in-g}$.

As can be seen from Figure 6-2 (a), the harvested solar energy follows a decreasing trend from $126\ \mathrm{kWh/(m^2 \cdot year)}$ in the first year to $85\ \mathrm{kWh/(m^2 \cdot year)}$ in the 15th year. On the contrary, the required energy for anti-icing follows an increasing trend from $70\ \mathrm{kWh/(m^2 \cdot year)}$ to $77\ \mathrm{kWh/(m^2 \cdot year)}$ over 15 years. One reason for variation of the harvested and required energies over time is the temperature change in the domains of HHP and HGHE, see Figure 6-2 (b). As can be seen, the average temperatures of domains rise over time. For the HHP system, the average temperature of the domain rises steadily from 3.4 ℃ in the first year to 4.4 ℃ in the 15th year. For the domain of HGHE, the temperature variation is sharper, so as the temperature increases from 3.8 ℃ in the first year to 9.2 ℃ in the 15th year. As the temperatures of domains increase, in particular the temperature of the HGHE domain, the energy difference between the harvesting and heating periods decreases, see Figure 6-2 (a). For the first year, this difference is $56\ \mathrm{kWh/(m^2 \cdot year)}$ and for the last year this difference is $8\ \mathrm{kWh/(m^2 \cdot year)}$.

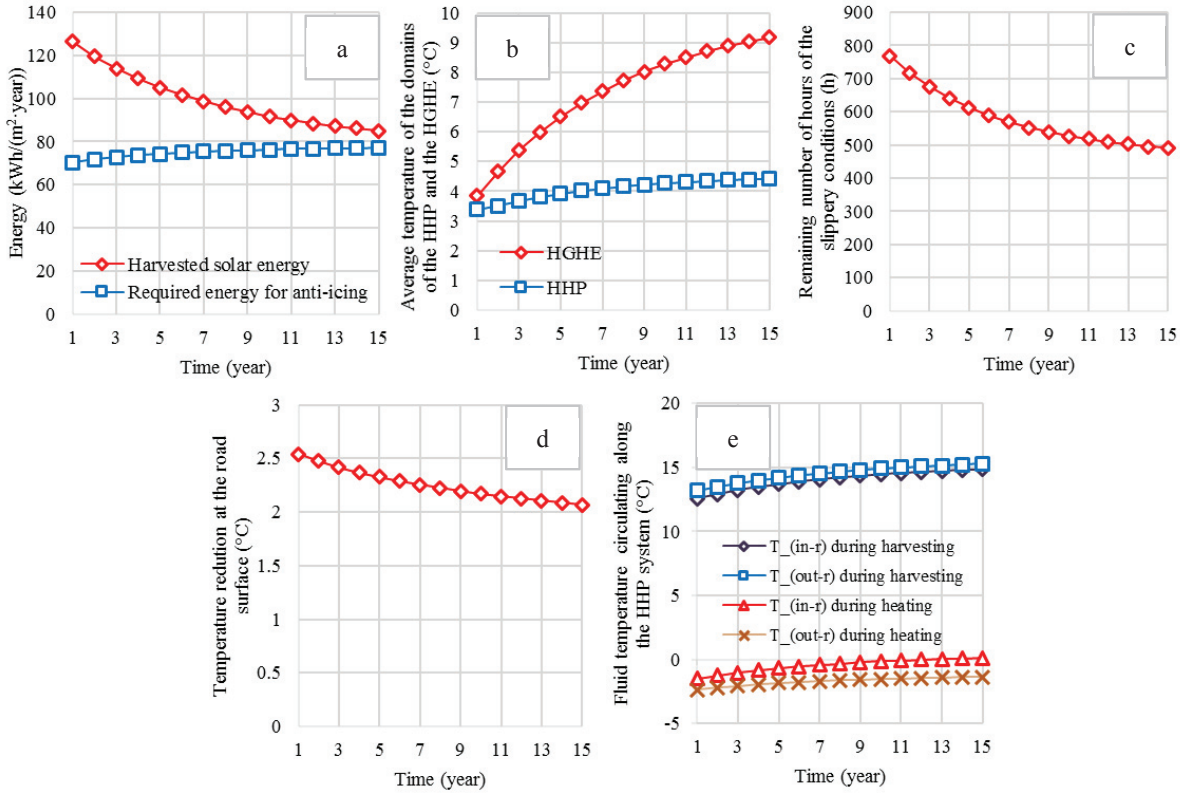

Figure 6-2. The results associated with the coupled HHP system to the HGHE (a) the harvested solar energy and the required energy for anti-icing (b) the average temperature through the domains of the HHP system and the HGEH, (c) the remaining number of hours of the slippery conditions on the road surface (d) the temperature reduction on the road surface and (e) the inlet and outlet temperatures during harvesting and heating periods.

As can be seen from Figure 6-2 (c), the remaining number of hours of the slippery conditions on the road surface decreases from 770 h to 485 h over 15 years. The reduction in the number of hours of the slippery conditions corresponds to the increase in the required energy for anti-icing the road surface, see Figure 6-2 (a). For the last five years, from the 11th year to 15th year, the average value of remaining number of hours of the slippery conditions is 498 h with the standard deviation of 11 h. For this period, the average value of the required energy for anti-icing is 76.3 $\mathrm{kWh/(m^2 \cdot year)}$ with the standard deviation of 0.3 $\mathrm{kWh/(m^2 \cdot year)}$.

Figure 6-2 (d) shows the temperature reduction on the road surface at the control point, see Figure 5-1. As can be seen, the temperature reduction on the road surface follows a decreasing trend from 2.6 ℃ in the first year to 2.1 ℃ in the 15th year. This reduction occurs due to the increase in the inlet temperature of fluid over time. As can be seen from Figure 6-2 (e), the inlet temperature of fluid, circulating along the HHP system, during harvesting period increases from 12.6 ℃ to 14.9 ℃ over 15 years. Based on Equation 6-2, the outlet temperature of fluid is always higher than the inlet temperature during harvesting period. For this period, the inlet temperature of fluid increases from 13.2 ℃ in the first year to 15.3 ℃ in the 15th year. Furthermore, Figure 6-2 (e) shows the inlet and outlet temperatures of the fluid during heating period. The inlet temperature of fluid during this period varies from -1.5 ℃ to $+0.12$ ℃ and the outlet temperature varies from -2.4 ℃ to -1.4 ℃ over 15 years. It should be noted that even if the fluid temperature is below 0 ℃, it is able to keep the temperature of the road surface above the

dew-point temperature and consequently prevents ice-formation on the road surface due to condensation.

6.3. Heat loss from the HGHE to the surrounding ground

This section presents the heat loss, flowing out from the HGHE to the surrounding ground. If it is assumed that: the same number of pipes embedded in the HHP system and the HGHE, the width of a lane of road is 3.5 m, the distances between the pipes in the HHP system is 0.1 m, the distance between the pipes in the HGHE is 2 m, then the width of the HGHE will be 70 m. In order to calculate the heat loss, a 2D numerical simulation model is created. To simplify the 2D numerical simulation model, it is assumed that the width of the surrounding ground is 70 m as well. The boundary conditions at the surface and the bottom of the HGHE, the bottom of the surrounding ground and the further sides of the surrounding ground which are not connected to the HGHE are set to be adiabatic. Furthermore, the boundary conditions at the surface of the surrounding ground are simplified by an equivalent temperature, T_{eq} (℃) and an equivalent heat transfer coefficient h_{eq} $(\mathrm{W/(m^2 \cdot K)})$. see Section 4-2 of **Paper VII** for details about T_{eq} (℃) and h_{eq}.

The scheme of the HGHE surrounded by the grounds are shown in Figure 6-3. The domain of C-E-K-I presents the HGHE and the two domains of A-B-C-E and I-K-L-M present the surrounding grounds.

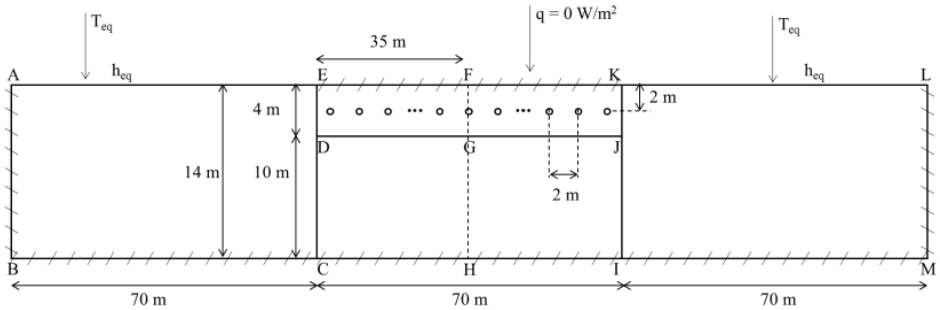

Figure 6-3. A scheme of the HGHE including surrounding grounds and boundary conditions.

To calculate the heat loss, the average heat flow per one meter of pipes, $q_{pipe}(\mathrm{W/m})$, is extracted from the hybrid 3D numerical simulation model of the coupled system. The heat flow of q_{pipe} has hourly values in line with the climate data and includes: the harvesting and heating periods as well as the period during which the harvesting/heating is off, $q_{pipe} = 0\ \mathrm{W/m}$. The values of q_{pipe} are used as the input data for the 2D numerical simulation model of Figure 6-3. The amount of energy loss during a year, E_{loss} $(\mathrm{kWh/(m^2 \cdot year)})$, is calculated as:

$$E_{loss} = \frac{2 \cdot L_g}{W_r \cdot L_r} \cdot \int_0^{1\ year} q_{surr} \cdot dt \qquad (6\text{-}4)$$

where q_{surr} $(\mathrm{W/m})$ is the heat loss from the HGHE to the surrounding ground, L_g (m) is the length of the HGHE, L_r (m) is the length of the HHP system and W_r (m) is the width of the HHP system. The constant value of 2 is used due to the symmetry in the numerical simulation. In this section, $L_g = L_r = 50$ m and $W_r = 3.5$ m.

Figure 6-4 (a) shows the results of E_{loss} associated with the domains of C-E-K-I, see Figure 6-3. As can be seen, the variation of E_{loss} versus time does not follow a constant trend, so E_{loss} increases from $3.9\,\mathrm{kWh/(m^2 \cdot year)}$ to $8.4\,\mathrm{kWh/(m^2 \cdot year)}$ over the first 10 years and then decreases to $8\,\mathrm{kWh/(m^2 \cdot year)}$ in the 15th year. Moreover, Figure 6-4 (a) shows the difference between the harvested and the required energies, $E_h - E_r$, versus time. As can be seen, the harvested solar energy is enough, even after heat loss, to use for anti-icing the road surface. Considering the heat loss from the domain of C-E-K-I, the harvested and required energies will reach to a balance in the 15th year, so as $E_h - E_{loss} = E_r$.

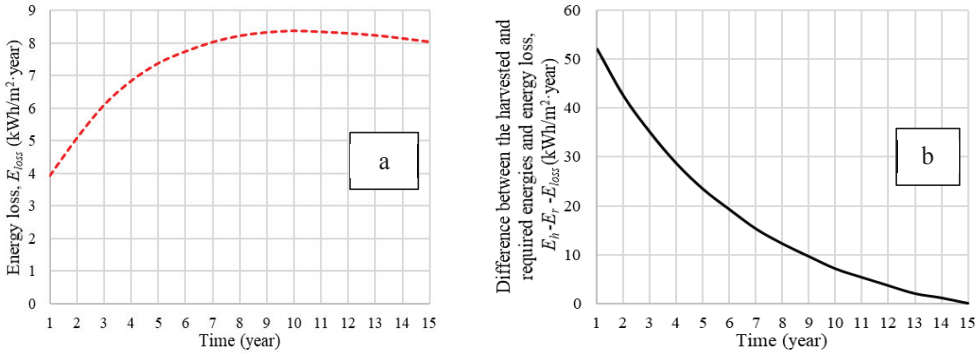

Figure 6-4. Variation of energy versus time (a) heat loss to the surrounding ground associated with the domain of C-E-K-I and (b) the difference between the harvested and the required energies.

6.4. The effects of the thermal properties of ground material

Thermal properties of the ground including thermal conductivity, density and specific heat capacity have a high contribution on the heat transfer between the pipes and surrounding soil [23]. In this section, the thermal properties of ground related to the HGHE are replaced with the thermal properties of clay [49], see Table 6-1.

Table 6-1. Thermal properties of the clay [49].

Material	**Thermal conductivity** $(\mathrm{W/(m \cdot K)})$	**Density** $(\mathrm{kg/m^3})$	**Specific heat capacity** $(\mathrm{J/(kg \cdot K)})$
clay	1.3	1460	880

The results related to the harvested and required energies, the remaining number of hours of the slippery conditions as well as the inlet and outlet temperature of fluid, circulating along the HHP system, during harvesting and heating periods are shown in Figure 6-5.

Replacing the thermal properties of the HGHE results in an approximately 30% increase in the harvested solar energy and an approximately 9% increase in the required energy for anti-icing the road surface. An increase in the required energy for anti-icing the road surface will result in a decrease in the remaining number of hours of the slippery conditions. Replacing the ground of the HGHE with clay results in approximately 210 h, on average, shorter remaining number of hours of the slippery conditions during a year. Furthermore, changing the thermal properties of the HGHE results in, on a 15-years average, a 1.6 ℃ reduction in the inlet temperature during the harvesting period and a 2.5 ℃ increase in the inlet temperature during the heating period.

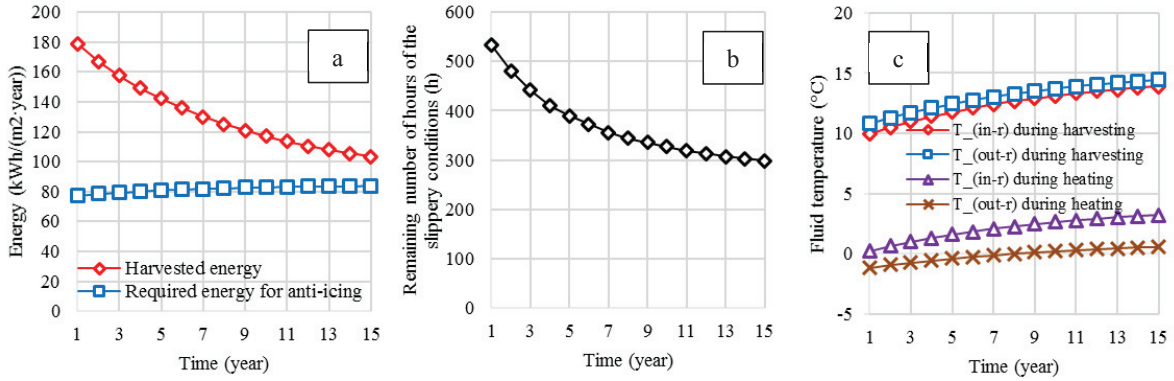

Figure 6-5. The results associated with the coupled HHP system to the HGHE, the thermal properties of which is replaced with values in Table 6-1 (a) the harvested solar energy and the required energy for anti-icing (b) the remaining number of hours of the slippery conditions on the road surface and (c) the inlet and outlet temperatures of fluid, circulating along the HHP system, during the harvesting and heating periods.

7. Summary and conclusion

The project of "safe and ice-free roads using renewable energy", aims at examining the possibility of utilizing harvested solar energy during summer for anti-icing the road surface during winter. In this thesis, five different steps were taken for studying this possibility. The first step was to determine the accurate thermal properties of three typical asphalt concretes used for the construction of roads in Sweden. The second step was to develop a 2D numerical simulation model, which was able to calculate the required energy for anti-icing the road surface and to obtain the remaining number of hours of the slippery condition on the road surface. The 2D model was a dynamic numerical simulation model, which was able to turn on/off the heating system based on the slippery condition on the road surface. However, the 2D model was not able to calculate the fluid temperature decline along the pipes and also not able to investigate the effects of the fluid flow rate on the efficiency of the HHP system. In order to solve this problem, a hybrid 3D numerical simulation model was developed. The hybrid 3D numerical simulation model was developed by serially connecting 2D numerical simulation model. The 2D models were connected to each other through the convective heat transfer along the pipe. Moreover, the hybrid 3D numerical simulation model was used: (i) to obtain the minimum required energy for totally preventing ice formation on the road surface and (ii) to investigate the feasibility of the coupled HHP system to the HGHE.

The obtained results in this study can be summarized as:

a) Thermal property of asphalt concrete:

The thermal conductivity of the asphalt concretes varies from 1 W/m·K to 3 W/m·K, depending on the aggregates type, bitumen content and air voids. The thermal conductivity of the asphalt concrete will increase by decreasing the air void content and using aggregates with higher thermal conductivities.

b) 2D numerical simulation model:

Using the 2D numerical simulation model, it was obtained that the annual required energy for anti-icing the road surface is 75 $\mathrm{kWh/(m^2 \cdot year)}$ and the remaining number of hours of the slippery condition is 128 h. It is important to mention that for running the 2D numerical simulation model of the HHP system, the fluid temperature was set to be 6 ˚C constant during which the heating system was turned on. The control point for checking whether the road surface is slippery or not was located on the road surface between two pipes.

c) Hybrid 3D numerical simulation model:

Using the hybrid 3D numerical simulation model of the HHP system and setting the inlet temperature of the fluid to 6 ˚C, it was obtained that the annual harvested solar energy considering to $T_{limit} = 6$ ℃ is 290 $\mathrm{kWh/(m^2 \cdot year)}$, the annual required energy for anti-icing the road surface is 84 $\mathrm{kWh/(m^2 \cdot year)}$, the remaining number of hours of the slippery condition is 217 h, the average outlet temperature of the fluid during harvesting period is 6.8 ˚C and that during anti-icing period is 2.3 ˚C. For running the hybrid 3D model of the HHP system,

the control point, for checking whether the road surface is slippery or not, was located on the road surface between two pipes above the outlet section.

Using the 3D numerical simulation model of the BTES with 20 boreholes and 200 m depth and analyzing the temperature increase/decrease at the borehole walls, it was obtained that the BTES can operate consistently and reliably on long term if the annual harvested solar energy in summer is higher than the annual required energy for anti-icing the road surface in winter. For the inlet fluid temperature lower than or equal to 12 ℃, the harvested solar energy was higher than the required energy for anti-icing the road surface.

d) Minimum required energy for anti-icing the road surface:

The superposition principle is used to separate the numerical simulation model into two fundamental sub-models: (i) a model with supplying heat to the HHP system and (ii) a model without any heat supply. A linear programming optimization was applied to obtain the minimum required energy for anti-icing the road surface. Furthermore, the maximum heat flux supplied to the HHP system is constrained to be 200 $\mathrm{W/m^2}$. The results showed that the minimum annual required energy for anti-icing the road surface is 107 $\mathrm{kWh/(m^2 \cdot year)}$. Supplying this amount of energy to the HHP system results in remaining only three hours of slippery conditions on the road surface.

e) Feasibility of the coupled HHP system to the HGHE:

A hybrid 3D numerical simulation model is used to simulate the coupled HHP system to the HGHE. The simulation model is run for 15 years to find out the long-term operation of the coupled system. A 2D numerical simulation model of the HGHE and the surrounding soil was created to obtain the heat loss flowing out from the storage to the surrounding ground.

The results showed that the harvested solar energy is enough for heating the road surface even after heat loss. The amount of harvested solar energy during summer is, on average, 100 $\mathrm{kWh/(m^2 \cdot year)}$. Less than 10% of this energy is lost to the surrounding ground. In addition, the required energy for anti-icing the road surface is 75 $\mathrm{kWh/(m^2 \cdot year)}$. Applying this amount of energy for anti-icing the road surface results in remaining of 580 hours of slippery conditions on the road surface, on an annual average.

8. Some suggestions for future work

In this thesis, the maximum obtained thermal conductivity of asphalt concrete was 3 W/(m·K) using the numerical model of the asphalt concrete microstructure. The future study can investigate the possibility of enhancing the thermal conductivity of asphalt concrete. For example, it should be examined how using slag aggregates to fabricate asphalt concrete can influence the thermal conductivity.

In this thesis, the effects of different parameters related to the HHP system were examined on the anti-icing performance of the HHP system. However, the investigation was done individually for each parameter. In future work, it is necessary to find out the combined effect of the parameters on the efficiency of the HHP system, e.g. the influence of enhancing the thermal conductivity of road layers and reducing the fluid temperature on the efficiency of the HHP system.

The HHP is a large-scale infrastructural system, for which, its sustainability is important from different aspects such as environmental impacts, road safety and lifecycle cost. Future studies should investigate the evaluation of economic and environmental performance of the HHP system by means of environmental Life Cycle Assessment (LCA) and economic Life Cycle Cost Analysis (LCCA).

Furthermore, the mechanical performance of the HHP system under the traffic load is of interest subject to study. Installing the HHP system might cause damage to and even collapse of the road. For example, the pipes can burst under heavy traffic loads. The fluid, circulating through the pipes, will leak into the road and can result in damage to the road layers. Also, temperature difference between two points of the road, induced by the heating system, can cause thermal cracks.

Finally, the obtained data from the test site of Östersund will be of interest to validate the numerical simulation model and also to develop the HHP system performance under real conditions.

References

[1] Shaopeng W, Mingyu C, Jizhe Z. Laboratory Investigation into Thermal Response of Asphalt Pavements as Solar Collector by Application of Small-Scale Slabs. Appl Therm Eng 2011;31:1582–7. doi:10.1016/j.applthermaleng.2011.01.028.

[2] Santamouris M. Using Cool Pavements as A Mitigation Strategy to Fight Urban Heat Island-A Review of the Actual Developments. Renew Sustain Energy Rev 2013;26:224–40. doi:10.1016/j.rser.2013.05.047.

[3] Norem H. Selection of Strategies for Winter Maintenance of Roads Based on Climatic Parameters. J Cold Reg Eng 2009;23:113–35. doi:10.1061/(ASCE)0887-381X(2009)23:4(113).

[4] Elvik R. Does the influence of risk factors on accident occurrence change over time? Accid Anal Prev 2016;91:91–102. doi:10.1016/j.aap.2016.02.026.

[5] Andersson A, Chapman L. The use of a temporal analogue to predict future traffic accidents and winter road conditions in Sweden. Meteorol Appl 2011;18:125–36. doi:10.1002/met.186.

[6] Strandroth J, Rizzi M, Olai M, Lie A, Tingvall C. The effects of studded tires on fatal crashes with passenger cars and the benefits of electronic stability control (ESC) in Swedish winter driving. Accid Anal Prev 2012;45:50–60. doi:10.1016/j.aap.2011.11.005.

[7] Arvidsson AK. The Winter Model – A new way to calculate socio-economic costs depending on winter maintenance strategy. Cold Reg Sci Technol 2017;136:30–6. doi:10.1016/j.coldregions.2017.01.005.

[8] Vignisdottir HR, Booto GK, Bohne RA, Ebrahimi B, Brattebø H, Wallbaum H. Life Cycle assessment of Anti-and De-icing Operations in Norway. CIB World Build. Congr., Tampere: 2016, p. 441–54.

[9] Wåhlin J, Klein-Paste A. A salty safety solution. Phys World 2017;30:27–30.

[10] Knudsen F, Natanaelsson K, Arvidsson A, Kärki O, Jacobsen Á, Guðmundsson G, et al. Vintertjeneste i de Nordiske land. Statusrapport 2014 (in Norwegian). Norge: 2014.

[11] Asensio E, Ferreira VJ, Gil G, García-Armingol T, López-Sabirón AM, Ferreira G. Accumulation of de-icing salt and leaching in Spanish soils surrounding roadways. Int J Environ Res Public Health 2017;14. doi:10.3390/ijerph14121498.

[12] Anuar L, Amrin A, Mohammad R, Ourdjini A. Vehicle accelerated corrosion test procedures for automotive in Malaysia. MATEC Wev Conf 2017;90:№01040. doi:10.1051/matecconf/20179001040.

[13] Gáspár L, Bencze Z. Salting Route Optimization in Hungary. Transp Res Procedia 2016;14:2421–30. doi:10.1016/j.trpro.2016.05.285.

[14] Mirzanamadi R, Hagentoft C-E, Johansson P, Johnsson J. Anti-icing of road surfaces using Hydronic Heating Pavement with low temperature. Cold Reg Sci Technol 2018;145:106–18. doi:10.1016/j.coldregions.2017.10.006.

[15] Ramsey JW, Hewett MJ, Kuehn TH, Petersen SD. Updated Design Guidelines for Snow Melting Systems. vol. 105. ASHRAE Transactions Symposia, USA: 1999.

[16] Liu X, Rees SJ, Spitler JD. Modeling Snow Melting on Heated Pavement Surfaces. Part I: Model Development. Appl Therm Eng 2007;27:1115–24. doi:10.1016/j.applthermaleng.2006.06.017.

[17] Mirzanamadi R. Ice free roads using hydronic heating pavement with low temperature: Thermal properties of asphalt concretes and numerical simulations. Licentiate thesis, Chalmers University of Technology, Gothenburg, Sweden, 2017.

[18] Xu J, Wang RZ, Li Y. A review of available technologies for seasonal thermal energy storage. Sol Energy 2014;103:610–38. doi:10.1016/j.solener.2013.06.006.

[19] Lee JU, Kim T, Leigh SB. Applications of building-integrated coil-type ground-coupled heat exchangers - Comparison of performances of vertical and horizontal installations. Energy Build 2015;93:99–109.

doi:10.1016/j.enbuild.2015.02.020.
[20] Wang H, Jasim A, Chen X. Energy harvesting technologies in roadway and bridge for different applications – A comprehensive review. Appl Energy 2018;212:1083–94. doi:10.1016/j.apenergy.2017.12.125.
[21] Wei K, Li W, Li J, Wang Y, Zhang L. Study on a design method for hybrid ground heat exchangers of ground-coupled heat pump system. Int J Refrig 2017;76:394–405. doi:10.1016/j.ijrefrig.2016.12.020.
[22] Johnsson J. Winter Road Maintenance using Renewable Thermal Energy. Licentiate thesis, Chalmers University of Technology, Gothenburg (Sweden), 2017.
[23] Al-Ameen Y, Ianakiev A, Evans R. Thermal performance of a solar assisted horizontal ground heat exchanger. Energy 2017;140:1216–27. doi:10.1016/j.energy.2017.08.091.
[24] Pan P, Wu SP, Xiao Y, Liu G. A Review on Hydronic Asphalt Pavement for Energy Harvesting and Snow Melting. Renew Sustain Energy Rev 2015;48:624–34. doi:10.1016/j.rser.2015.04.029.
[25] Eugster WJ. Road and Bridge Heating Using Geothermal Energy. Overview and Examples. Proc. Eur. Geotherm. Congr., Unterhaching, Germany 30 May-1 June: 2007.
[26] Pahud D. Simulation Tool for the System Design of Bridge Heating for Ice Prevention with Solar Heat Stored in a Seasonal Ground Duct Store, User Manual. Lugano, Switzerland: 2008.
[27] Pahud D. Serso, Stockage Saisonnier Solaire pour le Dégivrage d'un Pont. Rapport Final (in French). Bern, Switzerland: 2007.
[28] Li K, Hong N. Dynamic heat load calculation of a bridge anti-icing system. Appl Therm Eng 2018;128:198–203. doi:10.1016/j.applthermaleng.2017.09.024.
[29] Bobes-Jesus V, Pascual-Muñoz P, Castro-Fresno D, Rodriguez-Hernandez J. Asphalt Solar Collectors: A Literature Review. Appl Energy 2013;102:962–70. doi:10.1016/j.apenergy.2012.08.050.
[30] Abbasi M. Non-skid Winter Road, Investigation of Deicing System by Considering Different Road Profiles. Master Thesis, Chalmers University of Technology, Gothenburg (Sweden), 2013.
[31] Mirzanamadi R, Hagentoft C-E, Johansson P. Hydronic Heating Pavement With Low Temperature: The Effect of Pre-Heating and Fluid Temperature on Anti-icing Performance. 9th Int. Cold Clim. HVAC Conf., Kiruna, Sweden: 2018.
[32] Côté J, Grosjean V, Konrad J-M. Thermal Conductivity of Bitumen Concrete. Can J Civ Eng 2013;40:172–80. doi:10.1139/cjce-2012-0159.
[33] Dawson AR, Dehdezi PK, Hall MR, Wang J, Isola R. Enhancing Thermal Properties of Asphalt Materials for Heat Storage and Transfer Applications. Road Mater Pavement Des 2012;13:784–803. doi:10.1080/14680629.2012.735791.
[34] Adl-Zarrabi B, Johnsson J, Mirzanamadi R. Hydronic Pavement Using Low Temperature Borehole Thermal Energy Storage. 2016 Word Congr. Adv. Civil, Environ. Mater. Res., Jeju Island, Korea: 2016.
[35] Gurobi Optimization Inc. Gurobi Optimizer 2017.
[36] Meteotest. Meteonorm: Meteonorm, Global Meteorological Database. Handbook part II: Theory, version 6.1. Bern (Switzerland): 2010.
[37] Test site E18. E18 Test-Site, Perfect Choice for Unique Road Research Station 2014. http://testsitee18.se/Default.aspx (accessed March 19, 2017).
[38] Wang H, Chen Z. Study of critical free-area ratio during the snow-melting process on pavement using low-temperature heating fluids. Energy Convers Manag 2009;50:157–65. doi:10.1016/j.enconman.2008.08.019.
[39] Liu X. Development and Experimental Validation of Simulation of Hydronic Snow Melting Systems for Bridges. PhD thesis, Oklahoma State University, 2005.
[40] Li B, Wu SP, Xiao Y, Pan P. Investigation of heat-collecting properties of asphalt pavement as solar collector by a three-dimensional unsteady model. Mater Res Innov 2015;19:S1-172-S1-176.

doi:10.1179/1432891715Z.0000000001398.
[41] Ou T, Hu Y, Gustavsson T, Bogren J. On the relationship between the risk of hoar frost on roads and a changing climate in Sweden. Int J Climatol 2018. doi:10.1002/joc.5974.
[42] Adl-Zarrabi B, Mirzanamadi R, Johnsson J. Hydronic Pavement Heating for Sustainable Ice-free Roads. Transp Res Procedia 2016;14:704–13. doi:10.1016/j.trpro.2016.05.336.
[43] Yüksel N. The Review of Some Commonly Used Methods and Techniques to Measure the Thermal Conductivity of Insulation Materials. Insul. Mater. Context Sustain., Published by INTECH; 2016.
[44] Gustafsson M. Instruction Manual of Hot Disk Thermal Constants Analyser Software version 5.9. Götenburg, Sweden: 2013.
[45] Dixon C, Strong MR, Zhang SM. Transient plane source technique for measuring thermal properties of silicone materials used in electronic assemblies. Int J Microcircuits Electron Packag 2000;23:494–500.
[46] Chen J, Wang H, Asce AM, Li L. Determination of Effective Thermal Conductivity of Asphalt Concrete with Random Aggregate Microstructure. J Mater Civ Eng 2013;27:1–9. doi:10.1061/(ASCE)MT.1943-5533.0001313.
[47] Chen J, Zhang M, Wang H, Li L. Evaluation of Thermal Conductivity of Asphalt Concrete with Heterogeneous Microstructure. Appl Therm Eng 2015;84:368–74. doi:10.1016/j.applthermaleng.2015.03.070.
[48] Pan P, Wu S, Xiao Y, Wang P, Liu X. Influence of Graphite on the Thermal Characteristics and Anti-Ageing Properties of Asphalt Binder. Constr Build Mater 2014;68:220–6. doi:10.1016/j.conbuildmat.2014.06.069.
[49] Bergman TL, Adrienne S. Lavine, Frank P. Incropera, DeWitt DP. Introduction to Heat Transfer. Six Editio. New York: Wiley and Sons; 2011.
[50] Andolfsson T. Analyses of Thermal Conductivity from Mineral Composition and Analyses by Use of Thermal Conductivity Scanner A Study of Thermal Properties in Scanian Rock Types. Geology department at Lund University, Master's thesis, 2013.
[51] Robertson EC. Report of Thermal Properties of Rocks. Virginia: 1988.
[52] Hagentoft C-E. Introduction to Building Physics. 1:7. Lund, Sweden: Studentlitteratur (Sweden); 2001.
[53] Hagentoft C-E, Roots P. Design Rules for Floor Heating System Using New Analytical Formulas. CESBP Cent. Eur. Symp. Build. Phys. BauSIM 2016, Dresden: 2016, p. 23–8.
[54] Jaeger JC, Chamalaun T. Heat flow in an infinite solid bounded internally by a cylinder. Aust J Phys 1966;19:475–88.
[55] Claesson J, Dunand A. Heat extraction from the ground by horizontal pipes: a mathematical analysis. Stockholm, (Sweden): Swedish Council for Building Research; 1983.
[56] Liu X, Rees SJ, Spitler JD. Simulation of a Geothermal Bridge Deck Anti-icing System and Experimental Validation. Proc 82nd TRB Annu Meet 2003:1–22.
[57] Bayer P, de Paly M, Beck M. Strategic optimization of borehole heat exchanger field for seasonal geothermal heating and cooling. Appl Energy 2014;136:445–53. doi:10.1016/j.apenergy.2014.09.029.
[58] You T, Wu W, Shi W, Wang B, Li X. An overview of the problems and solutions of soil thermal imbalance of ground-coupled heat pumps in cold regions. Appl Energy 2016;177:515–36. doi:10.1016/j.apenergy.2016.05.115.
[59] Banks D. An introduction to thermalgeology: Ground source heating and cooling. Second Edi. UK: John Wiley & Sons, Ltd; 2012.
[60] Karlsson H, Hagentoft C-E. Application of Model Based Predictive Control for Water-Based Floor Heating in Low Energy Residential Buildings. Build Environ 2011;46:556–69. doi:10.1016/j.buildenv.2010.08.014.